Confined explosions: The effect of compartment geometry

Elsevier Editorial System(tm) for Journal of Loss Prevention in the Process Industries
Manuscript Draft

Manuscript Number: JLP-D-16-00400R1

Title: Confined explosions: The effect of compartment geometry

Article Type: Full length article

Keywords: Blast wave; blast wave reflexions; confined explosions; industrial accidents; blast mitigation; finite element analysis.

Corresponding Author: Dr. Filipe Teixeira-Dias, BEng, MSc, PhD, Hab

Corresponding Author's Institution: University of Edinburgh

First Author: Francisco C Salvado

Order of Authors: Francisco C Salvado; Arikson J Tavares; Filipe Teixeira-Dias, BEng, MSc, PhD, Hab; João B Cardoso

Abstract: The detonation of explosives inside closed spaces, such as industrial facilities or naval vessels, is a very complex phenomenon mainly characterised by an enhancement of internal overpressures and wave reflexions. However, the phenomenon is relevant to the analysis of the effect of accidental or intentional explosions. Examples include, for example, oil and gas industrial facilities, where pressure waves may be generated from accidental explosions. The resulting damage will be affected by the shape and dimension of the compartment and its degree of venting plus the position and weight of the charge. The vulnerability of small buildings, vessels, trains or airplanes remain to be better understood particularly where the safety of passengers and operators is involved. Since the published experimental data on confined explosions is scarce, a numerical model is created to perform a parametric analysis that can provide engineers with guidance for the analysis of the destructive effects of detonations in small compartments in transportation systems or explosions in confined industrial spaces. A thorough validation process of the numerical model, based on published experimental data is described. Known empirical relations are compared with the results obtained and new methods to estimate the peak pressure in the compartment are proposed. Qualitative guidance has also been derived as a starting point to assist designers to think of solutions that enhance safety inside vehicles or buildings in the event of intentional or accidental detonations and explosions.

Confined explosions: The effect of compartment geometry

Francisco C. Salvado[a,c], Arikson J. Tavares[a], F. Teixeira-Dias[b,*], João B. Cardoso[a,d]

[a]*Department of Mechanical and Industrial Engineering*
Faculdade de Ciências e Tecnologia Universidade Nova de Lisboa (FCT), 2829-516 Caparica, Portugal
[b]*School of Engineering, The University of Edinburgh, Edinburgh EH9 3JL, UK*
[c]*Naval Research Centre (CINAV), Escola Naval Alfeite, 2810-001 Almada, Portugal*
[d]*UNIDEMI, Faculdade de Ciências e Tecnologia, Universidade Nova de Lisboa, 2829-516 Caparica, Portugal*

Abstract

The detonation of explosives inside closed spaces, such as industrial facilities or naval vessels, is a very complex phenomenon mainly characterised by an enhancement of internal overpressures and wave reflexions. However, the phenomenon is relevant to the analysis of the effect of accidental or intentional explosions. Examples include, for example, oil and gas industrial facilities, where pressure waves may be generated from accidental explosions. The resulting damage will be affected by the shape and dimension of the compartment and its degree of venting plus the position and weight of the charge. The vulnerability of small buildings, vessels, trains or airplanes remain to be better understood particularly where the safety of passengers and operators is involved. Since the published experimental data on confined explosions is scarce, a numerical model is created to perform a parametric analysis that can provide engineers with guidance for the analysis of the destructive effects of detonations in small compartments in transportation systems or explosions in confined industrial spaces. A thorough validation process of the numerical model, based on published experimental data is described. Known empirical relations are compared with the results obtained and new methods to estimate the peak pressure in the compartment are proposed. Qualitative guidance has also been derived as a starting point to assist designers to think of solutions that enhance safety inside vehicles or buildings in the event of intentional or accidental detonations and explosions.

Keywords: Blast wave, blast wave reflexions, confined explosions, industrial accidents, blast mitigation, finite element analysis.

1. Introduction

Confined explosions have been studied in the last three decades, thought not to the same extent as free air explosions. Although extensive work has been published on the effect of stand-off free-air explosions, mainly on civil

*Corresponding author: F.Teixeira-Dias@ed.ac.uk

infrastructures [1, 2, 3, 4, 5, 6], significantly fewer publications are available on explosions inside closed spaces such as tunnels, buildings, aircraft structures and vessels. The main reason for this resides on the added complexity of the analysis, making the blast environment very difficult to describe. Nonetheless, understanding confined explosions is highly relevant as the energy concentration in these cases is typically much higher than on a free air blast [7]. As an example, most offshore infrastructures do not incorporate specific explosion damage and loss prevention measures in their design, and explosions, either accidental or intentional, may occur. Analytical and numerical tools will help in the evaluation of the threat and the vulnerability of some of those vessels.

In confined explosions, depending on the degree of venting, the early time-blast phenomena will be similar to a free air spherical or hemispherical burst. However, gaseous products will remain trapped in the closed space and the shock wave will be reflected from the boundaries of the compartment until the energy of the explosion is dissipated into heat. Reflected waves will propagate and interact with other surfaces generating more reflected waves. After a peak overpressure the high pressure and temperature gases will expand throughout the space in a more lengthy process. This is known as the gas pressure phase, where pressure will decay to ambient pressure as the gases cool down or leakages occur [8]. The initial pressure peak will be followed by a series of lower pressure reflections and the average pressure curve will decay towards the initial ambient pressure.

The equivalent TNT charge mass, the volume of the room V_i, the internal exposed area A_w, the ambient pressure P_a and the vented area A_i, if it exists, are the main parameters that affect the resulting internal pressure. The volume plays an important role as the confinement will cause an increase in pressure which in turn will increase the rate of the combustion causing an increase in temperature and again an increase in pressure, and so on until the peak overpressure for internal blast is reached. however, other parameters are the geometry of the compartment and the location of the explosive. This makes empirical predictions very difficult due to the lack of suitable empirical models contemplating so many combinations of different parameters. Excluding experiments, which are unpractical for design purposes, numerical methods are the most appropriate tool for these problems as long as validation of the methods and models can be ensured. Lagrangian methods that use empirical blast curves based on experimental data [9] are not appropriate in confined spaces as these methods cannot model reflections. To allow for a complete modelling of incident and reflected waves travelling along the full length of the compartment the Arbitrary Lagrangian-Eulerian (ALE) method is more adequate. This study shows that this can be a useful approach to the analysis of the effects of the detonation of high explosives (HE) inside closed structures.

2. Confined explosions

Structures exposed to a blast from the detonation of the same mass of explosive at the same stand-off distance will experience different loads depending on the degree of the confinement of the surrounding space. The degree of venting of the compartment ranges from fully vented to unvented as shown in Figure 1, reproduced from the US Armed Forces jointly edited manual [10], which presents abacuses and curves for engineering calculations on blast loadings on confined structures.

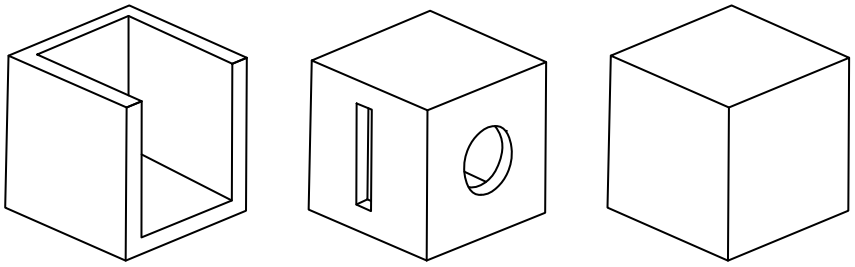

Figure 1: Schematic representation of the degree of venting of the blast from an explosion inside a compartment: (a) fully vented; (b) partially vented; (c) fully confined [10].

The pressure-time curve at a point near an explosion follows a Friedlander type curve, as shown in Figure 2. The positive duration of the curve will be longer in a confined explosion. In a fully confined blast the curve will tend asymptotically to a final equilibrium pressure higher than P_0. Consequently, the resulting impulse i_s, which is the area under the pressure-time curve, that is,

$$i_s = \int_{t_a}^{t_a+t_d} P(t)\mathrm{d}t \tag{1}$$

may be higher than that of a free-air burst, therefore imparting a more severe loading to the structure. It follows that the resulting damage may be potentially higher in confined explosions. However, Kinney et al. [11] reported that the damaging effect of a confined explosion may be less than expected due to the longer duration of the pulse, which may be larger than the critical response time of the structure. These authors also reported that peak overpressure is lower in confined unvented spaces and even lower if certain constituents are present, such as aluminium powder, which will be oxidised by the ambient air therefore diminishing the amount of oxygen available.

Relevant published work on confined explosions was published mostly in the 1970s [12, 13, 14, 15, 16] although research on the subject started earlier. Kinney et al. [11] used the following empirical relation between overpressure Δp [bar], mass W [kg] and confined volume V [m^3]

$$\Delta p = 13\frac{W}{V} \tag{2}$$

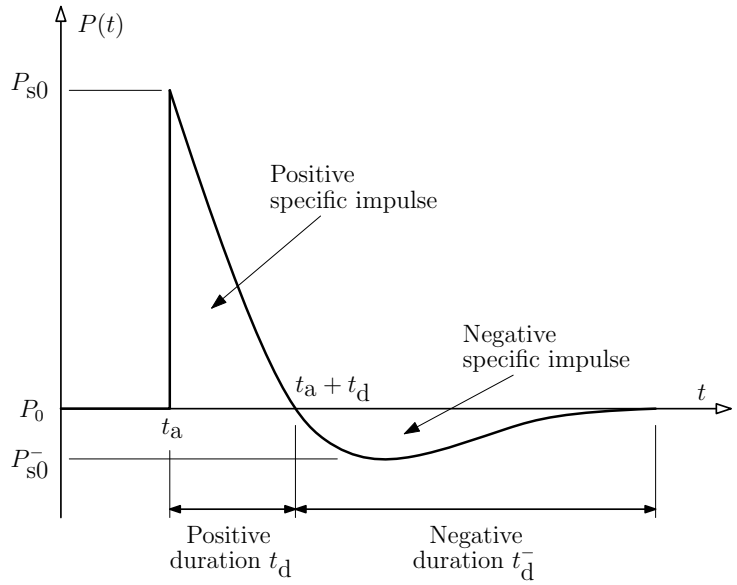

Figure 2: The Friedlander pressure-time curve $P = P(t)$.

referred to have been initially proposed in 1945 at the Los Alamos Scientific Laboratory, or, for adiabatic conditions and unvented spaces

$$\Delta p = 10^{-5}(\gamma - 1)\frac{H}{V} \tag{3}$$

although this equation greatly simplifies the phenomenon. H [J] is the heat of combustion and γ is the ideal gas ratio of heat capacities, usually $\gamma = 1.4$ for air at room temperature. Both equations provide only rough approximations to real data and improvements were later obtained through consideration of thermodynamic equilibrium and conservation equations. Pressure and temperature were obtained from the energy and enthalpy change that results from the reactions of the explosive constituents and the resulting products of combustion, applying the main balances of mass and energy, and the second law of thermodynamics. The compartment boundaries ensure adiabatic and rigid boundaries that avoid energy and mass dissipation [11, 17], which could affect the calculation of the peak overpressure. A very good agreement was found for TNT using these techniques, between experimental and calculated overpressures as a function of the ratio of the mass of explosive and the volume of air [kg/m^3].

Most contemporary studies consider the influence of the venting area on the value of peak pressures, with most publications producing a number of empirical equations meant to facilitate the design of safe suppressive structures [11, 14, 15]. Such empirical relations between overpressure and energy release are derived from experimental data, making it possible to calculate peak pressures and pressure decays for confined explosions as a function of an effective vented area. Design applications such as frangible covers [18] or exit tunnels in underground ammunition

storage facilities [19] benefitted from this early work. A comprehensive collection of empirical calculation methods for venting can be found in the works of Razus [20] and Tamanini [21] for gaseous deflagrations. The design of venting covers has been widely addressed as well. Molkov and co-workers [22, 23, 24] published a comprehensive study on venting considering various types of movable covers acted by the blast pressure. In a recent work, Feldgun [25] used experimental, analytical and numerical models to compare results for a cover or a free opening in a closed chamber. In both cases the pressure relief was observed to be similar. In the first instants, however, the chamber behaves as a fully confined room, before the cover moves sufficiently for the overpressure to drop to zero.

The use of computer codes has proved to be effective in these studies. Proctor [26] was one of the first to use them to study energetic reactions in closed structures, leading to the development of new codes such as INBLAST or BLASTINW in the early 1980s [27]. Numerical analysis and hydrocodes [28] were later used to calibrate the empirical equations and new semi-empirical methods were developed and incorporated into the US Tri-services manual [10]. Other authors [29, 30, 31] also used CFD codes to study venting effects on relief pipes. The location of the ignition point was found to have a strong effect on the measured peak pressures inside the chamber. Other aspect in favour of the use of numerical models is their ability to handle large scale and complex problems where experimentation is impossible, such as the assessment of blast damage in buildings [32].

Chan [33] used CFD to analyse wave reflexion phenomena inside an enclosure using an Eulerian mesh and validating his results with experimental data. The results showed that reflexions can continue for a significant amount of time and geometric symmetry in the enclosure can make multiple shock waves converge with strength comparable to the initial shock wave. Hu [34] used a commercial hydrocode to model the wave blast reflexions inside a closed prismatic box. The overpressure distribution profiles along a section of the box showed an increase at the corners and, in general, variations of length-to-depth ratios in a prismatic chamber were found to have a greater effect on the reflected overpressure. Edri [25] observed pressures 27% lower than those reported in the US Tri-services manual [10] on blast experiments in a closed chamber. Unexpectedly, the pressure at the corners of the compartment was also lower than at the centre of the walls. Sauvan [35] considered the influence of the walls of an almost closed volume around the explosive (for a chamber with no ceiling). The individual effects of each wall were then computed in terms of overpressures and pressure history. The interactions and reflexions originated by the walls were recorded by pressure sensors at each wall, leading to the conclusion that in semi-confined explosions the negative pressure phase can be as destructive as the positive. However, in the majority of other published results of blast wave experiments and numerical analyses this negative phase effect is not considered.

The structural effects of the internal blast on the compartment has also received attention from researchers. Whenhui [36] presented an analysis of the dynamic behaviour of a cylindrical explosive chamber and Auslender [37] and

Duffey [38] did a similar study albeit considering an elastic-plastic sphere. Confined explosions in cylindrical vessels have often been used to provide data on different explosive charge shapes. Wu [39] compared results of enclosed explosions in a blast chamber with data from the US Tri-services manual [10], with the latter reported to be under-predicted for horizontally oriented cylindrical charges.

A significant number of references look at the response of cylindrical vessels to internal blast although more focused on the deflagration phenomena due to the type of the contents that they normally carry, which constitutes another field of investigation dealing with explosion hazards in the chemical, oil and gas industries and in all sites where fuel vapours and gases can be accidentally ignited. Langdon [40] and Ma [41] studied the detonation of HE inside cylindrical vessels. Gaseous products and dust also constitute a potential source of hazard in the industry and an important number of studies have been published on the deflagration of these products in confined spaces, attempting to understand the effects of vents, obstacles and of chamber geometry [42, 43, 44, 45]. Generically, it can be concluded that the existence of ducts strongly enhances the vented explosion.

Confined explosion analysis can also be applied to urban areas, tunnels, underground stations were complex city and infrastructure geometries will constrain the flow of blast waves. Reflexions and channelling effects generated between the buildings [46], particularly at crossroads in the proximity of tall buildings, may result in overpressure time histories similar to an explosion in a confined space with openings. Results show that the blast effects in buildings can be both enhanced or attenuated by the presence of other buildings. An assumption of uncoupling between wave propagation and reflexion from the buildings has been reported to lead to reasonably accurate results, unless the facade has a large glazed area in which case the leakage will decrease the reflected pressures. Sklavounos and Rigas [47] used CFD to study this problem with a model based on three parallel obstacles perpendicular to the wave front. One of the interesting findings was the fact that structures surrounded by other structures will suffer more than if exposed to a single shock impact, which may result in extensive damages.

More recent studies on confined blast confirm the growing interest in the field. Geretto [48] presented a comparison of the maximum plate deflection resulting from various degrees of confinement in an enclosed explosion, showing that the structural deflection increases with the degree of confinement, contradicting the observations of Kinney [11] in 1979. Dragos [49] derived an equivalent idealised load from experimental pressure curves inside a closed space subjected to a confined explosion. This author proposed a simplified load curve that can be incorporated into structural response analysis tools, such as pressure-impulse diagrams. Benselama et al. [50] did three-dimensional simulations of rigid and closed box configurations inside which an explosive charge detonates, and the simulation of the propagation of a blast wave inside a tunnel with bifurcation. It was found that, in confined domains, the flow remains supersonic a long distance from the blast charge. The bifurcation led to a reduction in the overpressure inside the main pipe while

the overpressure inside the secondary pipe was weaker and the flow transonic. As expected, the results for the closed chamber showed an increase both in the peak pressure and in the reflexions from the compartment walls.

More recently Zyskowsky et al. [51] considered an explosion inside a closed rigid box, using Autodyn, a commercial hydrocode, and compared it with experimental data. Overpressure curves were produced at selected locations of the internal surface of the box. Price [52] also predicted the pressure-time history for specified locations in a canopy consisting of a roof deck suspended over a ceiling deck forming an attic space, using a three-dimensional shock wave physics code (CTH). The main aim was to look at the propagation of a blast wave through an opening to analyse interior wave reflexions. He found that better results were obtained for compartments with height to width ratios close to unity.

Most authors neglect the effects of afterburning and the main reason for this may be due to not only the analytical complexity of the phenomenon but also the difficulty in accessing adequate and efficient simulation tools. Until recently hydrocodes would assume that all the energy of the explosion is released upon detonation and used to drive the shock front forward. This, however, may not be a reasonable approach for under-oxidised explosives, as in these cases afterburn may act as a significant extra source of released energy. TNT, for example, which is about 73.9% oxygen deficient, will release about twice as much energy in the afterburn phase than in the detonation phase [53].

Earlier work [11, 13, 17, 26] studied the effect of the ratio between the mass of explosive and the volume of the compartment in confined detonations, having concluded that the increase in this ratio leads to an increase in the peak pressure and an increased residual pressure would result from a confined explosion. However, no consideration has been given to pressure variations in the peak pressures due to the shape of the compartment or due to different positions of both of the detonation point and the point of pressure measurement. More recently afterburning became a significant topic of interest. A brief review can be found in the report by Sherkar and co-workers [6]. Some simplifying methods have recently been proposed to ease the numerical simulations which are known to be lengthy and not cost efficient. An example of such a method includes shifting of the normal pressure-time curve, obtained without considering afterburning, by an amount proportional to the rate of the total explosive energy release to the heat of detonation [54, 55, 56]. It is expected that more attention will be given to the phenomena as some commercial hydrocodes now include means to simulate afterburning [57] which were not available until recently.

An important parameter of the analysis is the rate of release of afterburn energy, which often follows complex thermodynamic models [58] or is simply assumed as an additional constant or linear term in the equation of state of the explosive in hydrocodes that possess this feature [57]. The heat of the reaction to be considered in the hydrocodes can be derived from the molar mass of explosive and the available oxygen. Heats of reaction for afterburning of well known explosives are available in the literature [59, 60] or can be obtained by using thermo-equilibrium codes such as

CHEETAH [61] or CEA [62]. Salzano refers to the use of the Le Chatelier diagrams for explosives as a very promising alternative to the use of the classical equations of state [53]. From these diagrams it is possible to obtain the afterburn pressure as a function of the explosive/air mass-volume ratio.

This brief review shows the added complexity of a confined explosion, which involves reflexion and interaction of blast waves. The published information on internal blast simulation is still scarce although some parametric analyses are available [34] and recent publications show a growing interest in the field.

3. Numerical model

Setting-up experimental tests for confined explosions is more complex than for free-air explosions. Numerical simulations, however, can be used to rapidly accommodate different geometries, HE (mass, material, etc.), stand-off distances, that otherwise would require building different test devices. Hydrocodes are widely used for the purpose of analysing high-pressure, high-velocity, dynamic, transient phenomena [63] and one of such commercially available codes is LS-DYNA, from the Livermore Software Technology Corporation (LSTC). LS-DYNA is a numerical analysis code that incorporates different methods to study explosive blast phenomena. Amongst these, the Arbitrary Lagrangian-Eulerian (ALE) approach is reported to have been successfully used in numerical simulation of high-explosive detonations and blast waves. ALE mathematical foundations are well documented [64, 65, 66, 67] and the method has been further developed to overcome the difficulties that arise from large mesh distortions. It is based on an arbitrary movement of a reference computational domain (the initial mesh position) in relation to both a material domain (the initial material position) and a spatial domain (the current configuration). This relative movement of the computational mesh reduces element distortion of an otherwise Lagrangian mesh. In a fully Eulerian approach, which is a particular case of the ALE formulation, the computational domain will remain fixed and coincident with the spatial domain, completely eliminating element distortion. A multi-material formulation can be used to simulate the propagation of the reaction products of the detonation and the fluid-structure interaction problem where the fluid can be defined by more than one material. In an explosion problem an element may contain air and gas produced from the detonation of the explosive [68] and state variables will be obtained by adequate weighing of the respective values for each of the two materials present in the element.

3.1. Multi-Material ALE formulations

The Navier-Stokes equations need to be integrated in time, together with boundary conditions, if the solution for the flow of the products of the explosion is to be found. A major simplification can be done by considering the reference mesh fixed in space, that is considering an Eulerian approach. This removes the need for a re-meshing and

smoothing process albeit maintaining the complexity of the time integration procedure. A split approach [65] has been implemented in LS-DYNA to simplify the problem. In this split approach each time-step is divided in two: a Lagrangian step and an advection step. The Navier-Stokes equations are

$$\frac{\partial \rho}{\partial t} + \nabla \cdot (\rho \mathbf{v}) = 0$$

$$\frac{\partial \rho \mathbf{v}}{\partial t} + \nabla \cdot (\rho \mathbf{v} \otimes \mathbf{v}) = \nabla \cdot \sigma + \mathbf{f} \tag{4}$$

$$\frac{\partial \rho E}{\partial t} + \nabla \cdot (E \mathbf{v}) = \sigma : \nabla \mathbf{v}$$

where ρ is the density, $\mathbf{v}$ is the flow velocity, $\mathbf{f}$ is the vector of externally applied forces, E is the total (internal and kinetic) energy and σ is the total Cauchy stress tensor, given by

$$\sigma = -p\mathbf{I} + \mu \nabla \mathbf{v} + \nabla \mathbf{v} \tag{5}$$

In the above equation, p is the pressure, $\mathbf{I}$ is the identity tensor and μ is the dynamic viscosity. Equations (4) can be rewritten generically as

$$\frac{\partial \phi}{\partial t} + \nabla \cdot \Phi = \mathbf{S} \tag{6}$$

where

$$\phi = \begin{bmatrix} \rho \\ \rho \mathbf{v} \\ \rho E \end{bmatrix}, \qquad \Phi = \begin{bmatrix} \rho \mathbf{v} \\ \rho \mathbf{v} \otimes \mathbf{v} \\ E \mathbf{v} \end{bmatrix} \qquad \text{and} \qquad \mathbf{S} = \begin{bmatrix} \mathbf{0} \\ \nabla \cdot \sigma + \mathbf{f} \\ \sigma : \nabla \mathbf{v} \end{bmatrix} \tag{7}$$

Mass conservation is assumed in its integral form

$$\rho J = \rho_0 \tag{8}$$

rather than the equation of continuity [67] because of its simplicity and better accuracy to compute the current density ρ. ρ_0 is the initial density and J is the volumetric strain given by the Jacobian

$$J = \det\left(\frac{\partial x_i}{\partial X_j}\right) \tag{9}$$

The splitting approach consists of separating the Eulerian conservation Equation (6) in two terms: a source and a convective term, which are, respectively

$$\frac{\partial \phi}{\partial t} = \mathbf{S} \tag{10}$$

$$\frac{\partial \phi}{\partial t} + \nabla \cdot \Phi = \mathbf{0} \tag{11}$$

The source equations (10) are the Lagrangian conservation equations, corresponding to the Lagrangian step. The convective equations (11) describe the transport phenomena and can be referred to as the Eulerian step. In the split approach the two steps are solved separately and sequentially to calculate velocity and internal energy. In the Lagrangian step the stresses are calculated at the integration points and nodal accelerations, velocities and displacements are then obtained with an explicit time integration scheme. The mass is assumed to be lumped at the nodes, which leads to a diagonal matrix which simplifies the calculation of the accelerations.

In the second step the resulting distorted mesh is remapped onto an arbitrary position in the case of an ALE mesh, or to its previous position for an Eulerian description. The advection problem will then be solved using a finite volume procedure. State variables can thus be mapped onto the rezoned mesh. An advection scheme is necessary to calculate the material fluxes. This can be done using one of three methods: the first order accurate upwind Donor Cell (which is a first order Godunov method) [69], the second-order van Leer [70] and a first order accurate Donor Cell modified to conserve total energy over each advection step, instead of conserving only internal energy. LS-DYNA also combines these algorithms with the Half-Index Shift method [71] to find the advection of node-centred variables.

By using a Multi-Material ALE (MM-ALE) element formulation, the gaseous products of the explosion and the ambient air that initially fills the mesh can occupy the same elements. It is possible, using a suitable interface tracking algorithm, to follow the flow of both materials through the Eulerian mesh. This is a computationally demanding task and under-integrated elements will be used in this type of simulation. This calls for hourglass control as under-integrated elements do not account for the internal forces necessary to counter zero energy deformation modes, which tend to appear in these cases.

An additional set of equations has to be considered when solving these problems because, when pressures are significant, volumetric deformations will be large as well, and the hydrostatic component of the stress tensor becomes larger than the deviatoric stresses. As a consequence, a relation between pressure, volumetric deformation and energy is necessary, an equation of state (EOS). In the simulation of an explosion at least two EOS are needed, one for the explosive and another for the air. To simulate the high explosive detonation process the following Jones-Wilkins-Lee EOS is normally used [72]

$$P = A\left(1 - \frac{\omega}{R_1 V}\right)e^{-R_1 V} + B\left(1 - \frac{\omega}{R_2 V}\right)e^{-R_2 V} + \omega\frac{E}{V} \tag{12}$$

This is an empirical equation obtained from the expansion of the internal energy equation near the isentrope of the detonation products [73]. More details on its derivation can be found in the work of Alia and Souli [68].

For air, the following gamma law modelled by a linear polynomial equation (linear relative to the internal energy

E) has been used

$$P = C_0 + C_1\mu + C_2\mu^2 + C_3\mu^3 + E\left(C_4 + C_5\mu + C_6\mu^2\right) \tag{13}$$

where $\mu = (\rho/\rho_0) - 1$ and ρ/ρ_0 is the ratio of the current to the initial (reference) densities. Coefficients C_2 and C_6 are set to zero if $\mu < 0$. For an ideal gas the expression is reduced to

$$P = (\gamma - 1)\frac{\rho}{\rho_0}E_0 \tag{14}$$

as all coefficients will be made equal to zero except $C_4 = C_5 = (\gamma - 1)$ and $\gamma = c_p/c_v$ is the ratio of specific heats.

When refinement or problem scale are expected to make computations very lengthy, another available technique is mapping. For full scale domains were meshes will easily have millions of elements, the domain can be scaled using 2D to 3D mapping techniques [74]. Mapping is implemented in most commercial hydrocodes, including LS-DYNA, which allows analyses to be split into two phases. In the first phase a 2D mesh is used to initialise the detonation and the expansion of the reaction gases. This mesh has to be very refined to allow the development of a smooth wave front and a good set of energy results. Afterwards, the 3D problem is initialised with the input data calculated from the 2D analysis. The 3D mesh can be significantly coarser, which is the real advantage of the technique.

To ensure good overall results it is necessary that the 2D results are as good as possible. Some authors [75] compared results obtained with spherical and prismatic meshes. The first allow a much better definition of the blast wave. However, further away from the detonation point, the element aspect ratio increases and for aspect ratios in excess of ten pressures will tend to be overestimated. This imposes a practical limit in the mesh extent. Prismatic meshes may also suffer from some anomalies. Larcher [75] reported that peak pressure values are smaller along the diagonals of prismatic meshes. In the present study a regular square mesh of 200×200 [cm^2] with 250,000 elements was used and some differences were initially found for the peak pressure values at tracer points equally distant from the detonation point but at different azimuths. However, the higher peak pressure values were found along the diagonals, contradicting Larcher's findings [75]. These anomalies were minimised by using a delayed mesh relaxation technique and coincident readings of peak pressure were obtained both at the diagonal and at a point near one of the edges of the box-shaped mesh.

4. Numerical model validation

The optimal choice of modelling techniques and parameters to replicate the physical response of the system is known to be a complex task [76]. A thorough validation method was defined to ensure the proposed models were reliable. Three examples where experimental results were available in the literature were thus used for validation

purposes. These examples are described in the following sections. The high explosive used is C4, which is a mixture of Hexogen (RDX) with a plasticiser compound, often used in military applications. Air and explosive properties were adopted from Alia and Souli [68] and are listed in Table 1, where D is the detonation velocity and P_{CJ} is the Chapman-Jouguet pressure. E_0 and V_0 are the initial internal energy and the relative volume, respectively. The C_i coefficients are all set to zero except $C_4 = C_5 = \gamma - 1$. The material properties are listed in Table 1.

Table 1: Parameters for the EOS of explosive and air [68].

Material	C_1 [−]	C_2 [−]	C_3 [−]	C_4 [−]	C_5 [−]	C_6 [−]	C_7 [−]	E_0 [Mbar]	V_0 [−]	ρ_0 [g/cm^3]
Air	0	0	0	0.4	0.4	0	0	2.5×10^{-6}	1.0	1.293×10^{-3}

Material	A [Mbar]	B [Mbar]	R_1 [-]	R_2 [-]	ω [-]	E_0 [Mbar]	V_0 [-]	ρ_0 [g/cm^3]	D [cm/μs]	P_{CJ} [Mbar]
C4	5.98155	0.1375	4.5	1.5	0.32	0.087	1.0	1.601	0.804	0.281
TNT	3.7120	0.03231	4.15	0.95	0.30	0.07	1.0	1.590	0.693	0.210

4.1. Free air explosion

Alia and Souli [68] and Mahmadi and Aquelet [77] reported an experiment where a spherical charge of plastic explosive C4 was detonated in a mass of air at room temperature. These authors also used LS-DYNA to simulate the phenomenon. In the experiment the pressure peak was measured by a sensor placed 5 ft (152.4 cm) from the point of detonation. In LS-DYNA these pressure sensors can be simulated by means of tracer points defined at the sensor positions. The mass of the charge was 1 lb (454 g), corresponding to a sphere with radius 4.07 cm. Both papers [68, 77] present a comparison of numerical and experimental results and report a very good agreement in the time of arrival and only slightly different peak pressure values. These results are listed in Table 2 and were used for comparison and validation purposes in the present paper.

Table 2: Peak pressure and time of arrival (experimental and numerical) as reported by Alia and Souli [68] and Kamal and Aquelet [77]: (a) with a mesh of 27,972 elements and (b) with a mesh of 56,916 elements.

	Experimental		Numerical	
Source	Peak pressure [bar]	Time of arrival [ms]	Peak pressure [bar]	Time of arrival [ms]
Alia and Souli (2006) [68]	2.96	1.5	2.7 (a)	1.44
			2.9 (b)	1.50
Mahmadi and Aquelet (2008) [77]	3.406	—	3.405	—

All simulations were run with LS-DYNA R711 in the same machine. Different degrees of mesh refinement were used, namely 71,199 (mesh 1), 104,329 (mesh 2) and 147,649 (mesh 3) elements. Symmetry boundary conditions

were also adopted. Numerical parameters that were varied include the advection logic and the advection method. A mesh delaying relaxation option was also used to increase accuracy, as suggested by Mahmadi and Aquelet [77]. This contracts the mesh locally at the shock wave front. The geometry of the model — one-eighth of the domain modelled with a spherical mesh — is shown in Figure 3. The region where the explosive is has been greatly refined in comparison to the remaining mesh (see Figure 3) to allow for a better representation of the detonation process and development of a well-defined wave front.

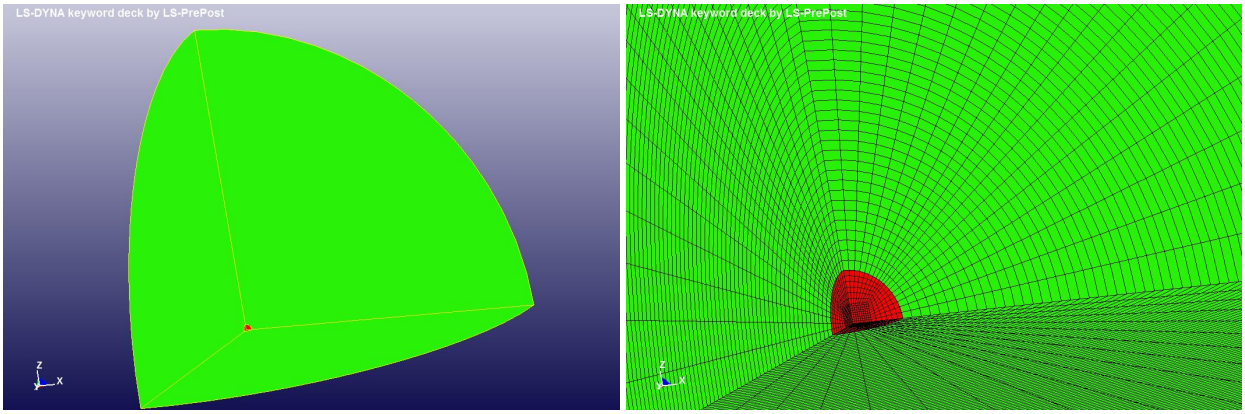

(a) (b)

Figure 3: Discretisation for the free air explosion model: (a) one-eighth of the domain and (b) detail of the spherical explosive charge (red) at the centre (mesh size 147,649 elements).

Figure 4 shows the pressure-time readings, for a 3D analysis, at the same tracer point for all the three considered meshes and two advection logics available in LSDYNA. For each mesh the advection method was also varied. It is immediately apparent that using the alternative advection logic (see Figure 4a) the pressure peaks are much lower than when using the default logic (see Figure 4b) and significantly different from the experimental result obtained by Alia and Souli [68]. The alternative method was thus abandoned. From the results in Figure 4b it can be seen that there is good agreement between the proposed numerical model and Alia and Souli's experimental results. From Figure 4b it can be concluded that the best pressure results were obtained when combining the Van Leer advection method and the most refined mesh or with the modified Donor Cell method and the intermediately refined mesh (peak pressure results were 2.9 and 3.0 bar, respectively). An even more refined mesh (255, 949 elements) was also used but, as mentioned above, results diverged excessively, unrealistic pressure curve shapes and values were found and thus this refined mesh was discarded. Consequently, in subsequent runs only advection methods 2 and 3 were applied as it was found that method 1 (the Donor Cell method) was not entirely satisfactory.

A second set of simulations of the same validation problem, albeit in two dimensions (2D), was run leading to good results for both advection logics. Results of the 2D analyses are listed in Table 3 and can be compared with

the reference experimental and numerical results in Table 2 [68, 77]. The optimal combinations of advection method and advection logic results are highlighted in Table 3 and it can be concluded that for this particular problem the default advection logic should only be combined with a first order Donor Cell advection method, whilst the alternative advection logic yields good results combined with a second order accurate (van Leer) advection method. Delayed relaxation [77] was found to be necessary in all 2D simulations in order to better match the numerical results to the experimental observations.

Table 3: Free air explosion: results obtained with 2D meshes and different advection logics and methods.

Number of elements in 2D mesh	Advection logic DCT	Advection method METH	Delayed mesh relaxation parameter PREF	Peak pressure at sensor [bar]	Time of arrival of shock wave [ms]
14,375 elements (quarter circle)	Alternative	Van Leer	Not used	4.90	1.25
	Alternative	Van Leer	0.01	6.00	1.13
	Alternative	M. Donor Cell	Not used	4.25	1.55
	Alternative	M. Donor Cell	0.01	5.20	1.25
	Default	Van Leer	Not used	2.64	1.52
	Default	Van Leer	0.01	2.93	1.46
	Default	M. Donor Cell	Not used	2.81	1.47
	Alternative	Donor Cell	0.01	2.92	1.44
250,000 elements (squared)	Default	M. Donor Cell	0.01	2.63	1.54
	Default	Van Leer	0.01	2.88	1.42
	Alternative	M. Donor Cell	Not used	4.69	1.30
	Alternative	Van Leer	Not used	5.52	1.23

4.2. Confined explosion I

The second example was used to validate the ALE methodology in the analysis of a confined explosion. Chan [33] published experimental data on a confined blast inside a rectangular steel bunker measuring 10×8×8 [ft^3]. The authors used 1 lb of C4 at the centre of the compartment and pressures were measured on three gages (front, left and corner). The location of the gages is shown in Figure 5. Mesh refinement is known to be a very important factor in ALE simulations but this may become unpractical for full scale domains such those described by Chan [33]. Consequently, a mapping technique was used to speed up the simulation whilst maintaining accuracy.

The obtained numerical results are shown in Figure 6 along with the experimental observations. The initial peak overpressures recorded at the front, left and corner gages were 600, 420 and 200 kPa, respectively (see Figures 6a to 6c). The equivalent numerical results are 667, 300 and 210 kPa. With the exception of the left gauge, there is good agreement between numerical and experimental values for both pressure and time of arrival. The overall pattern of the series of incident and reflected waves are in reasonable agreement with the numerical results, although a shorter time lag is observed. This may be due to the fact that in confined explosions the ambient air heats up and this affect

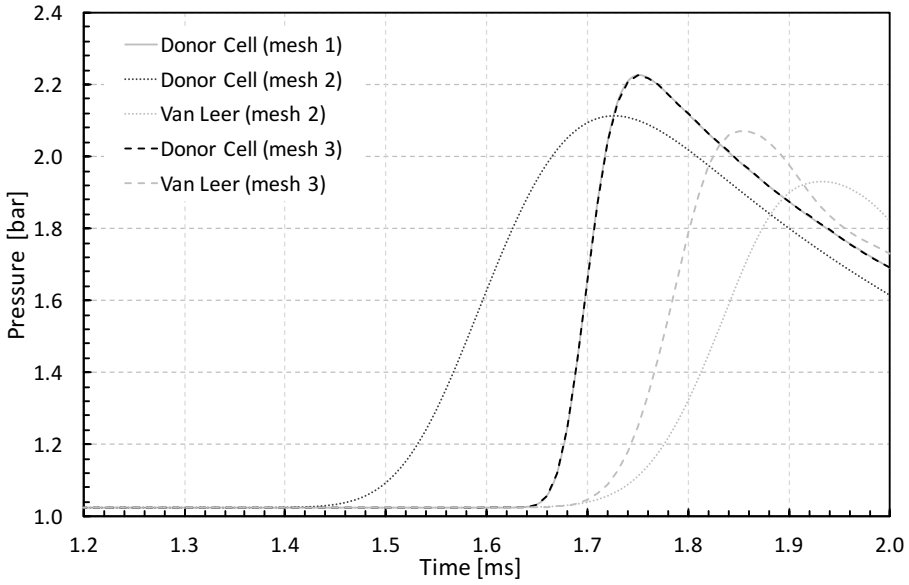

(a)

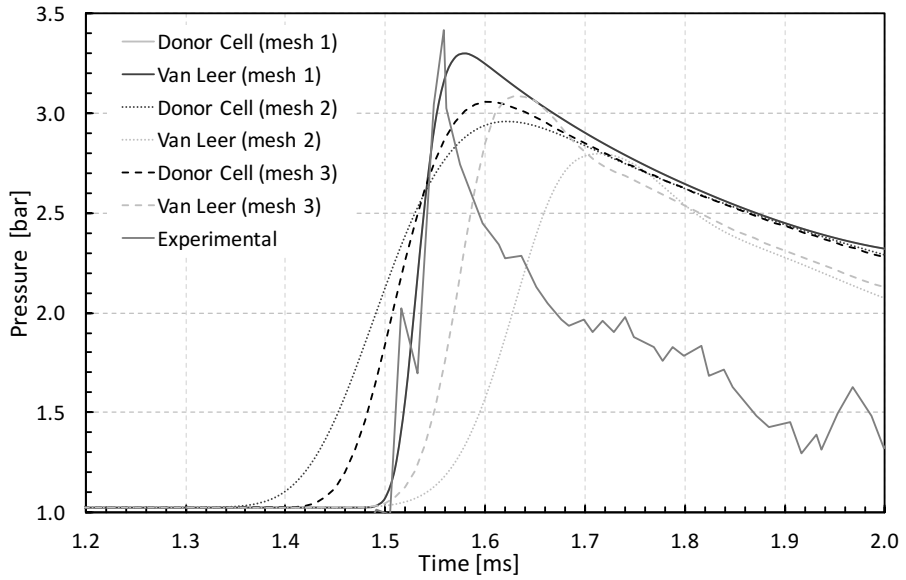

(b)

Figure 4: Numerical and experimental pressure curves read at the same tracer point using (a) the alternative advection logic and (b) the default advection logic.

the shock wave speed. Additionally, a ±20% error in the gauges was reported by Chan [33], which certainly adds to the observed discrepancies.

A mesh convergence analysis was done, resulting in a mesh with 1.25 million brick elements, corresponding to elements of approximately 2.4 cm in length, and all simulations were run on an Intel i7-2700K CPU at 3.5 GHz .

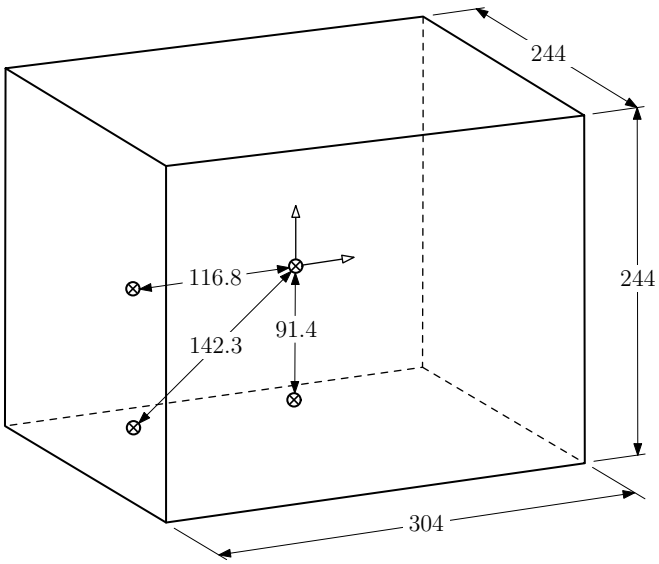

Figure 5: Dimensions (in [mm]) of the steel bunker and location of pressure sensors in the experiment of Chan [33].

4.3. Confined explosion II

The last validation example is based on the experiments reported by Zykowski [51], who measured blast wave pressures from the detonation of a mixture of oxygen and hydrogen in a small box (dimensions $50 \times 30 \times 40$ [cm^3]). Hu [34] used the ALE method to simulate the same experiment using AUTODYN relying on a single mesh of hexahedral elements and assuming rigid compartment walls. The present study replicated Hu's analysis in LS-DYNA albeit using the mapping technique. Under-integrated solid elements were used with the mesh sizes listed in Table 4, which also shows the box dimensions. The location of the detonation is $(x, y, z) \equiv (25, 0, 25)$ [cm] and the location of the sensor is $(x, y, z) \equiv (6, 25.5, 0)$ [cm], with the origin set at the lower corner of the box. More details can be found in Hu [34].

Table 4: Finite element mesh parameters for the simulation of a confined explosion in a closed rigid compartment.

	2D		3D	
Mesh	Size (x, y) [cm]	Element size [cm]	Size (x, y, z) [cm]	Element size [cm]
1	$(25, 30)$	0.02	$(50, 30, 40)$	0.625
2	$(25, 30)$	0.04	$(50, 30, 40)$	1.25
3	$(25, 30)$	0.08	$(50, 30, 40)$	2.5

The obtained peak pressure and time of arrival results are plotted in Figure 7 showing that the 1.7 bar peak pressure and the shape of the pressure history plot agrees well with both the experimental and numerical results reported by Hu [34]. The best results were found for mesh 1 with 245,760 elements. The mapping file was obtained running a

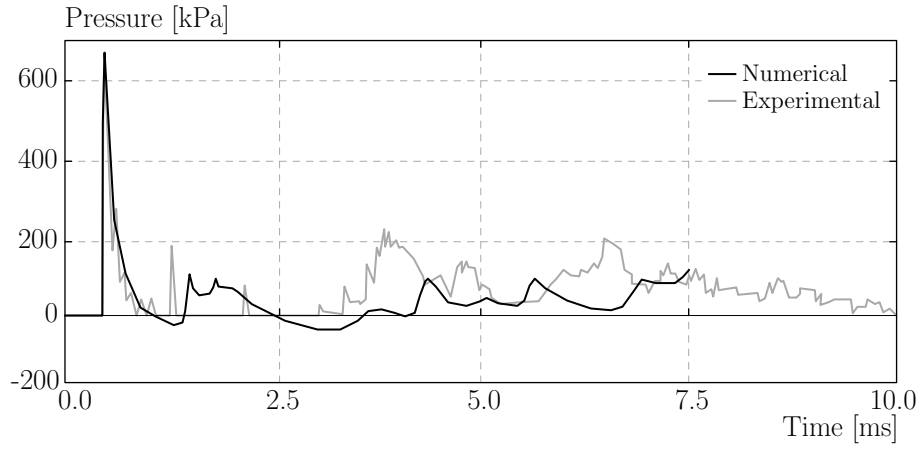

(a)

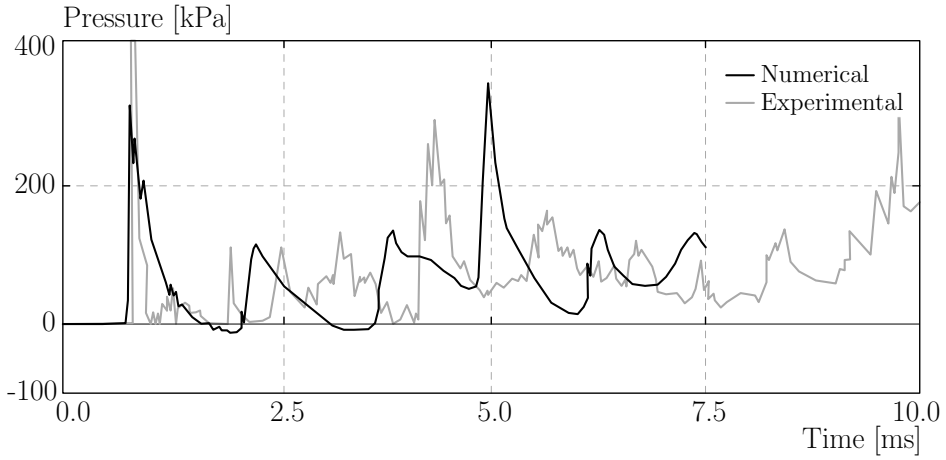

(b)

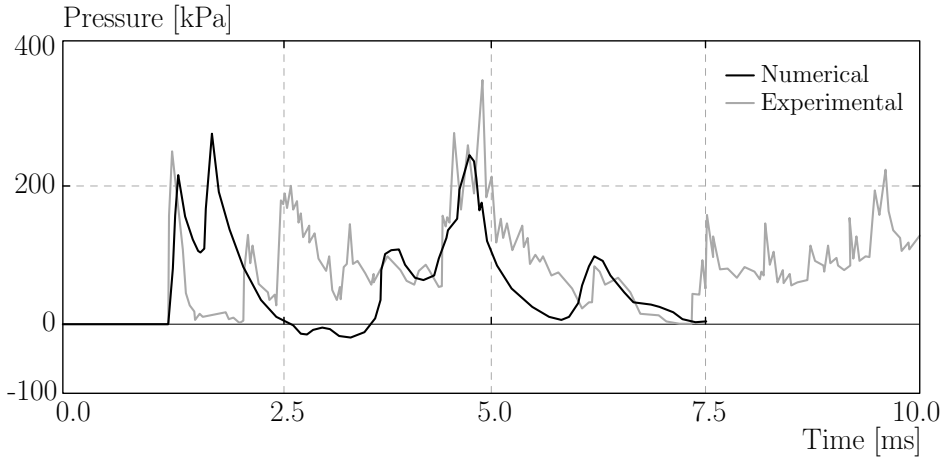

(c)

Figure 6: Calculated and measured [33] peak blast overpressures from a confined explosion inside in a closed steel bunker: (a) front sensor, (b) lateral sensor and (c) corner sensor.

2D rectangular mesh with 1,875,000 elements. Both advection methods (Van Leer and Modified Donor Cell) were tested and give similar results. However, the solution showed to be strongly influenced by the advection logic, as can be seen in Figure 8. The two solutions shown follow similar trends but differ in the peak pressures values.

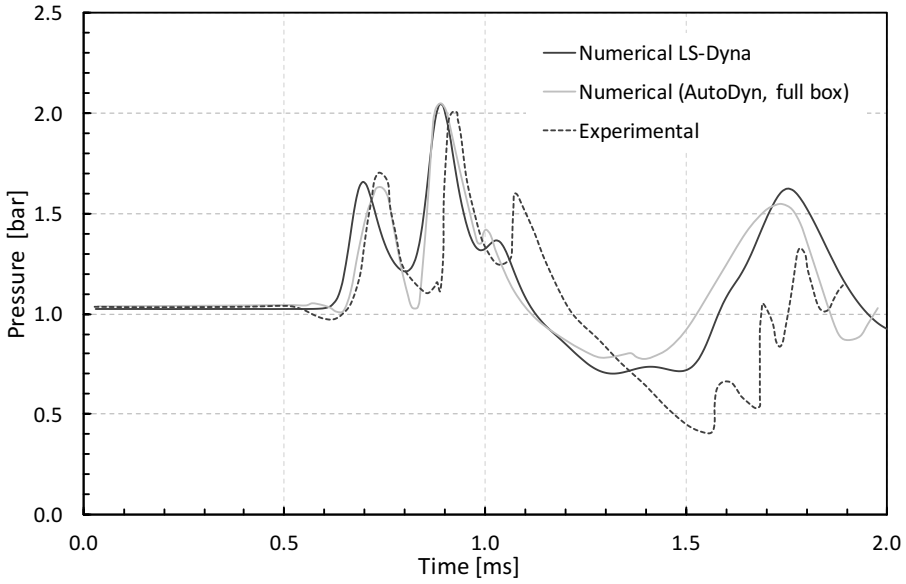

Figure 7: Comparison between numerical and experimental results. The alternative advection logic defined in LS-DYNA input has been used in the numerical curve. The AUTODYN and experiments curves were reproduced from Hu [34]

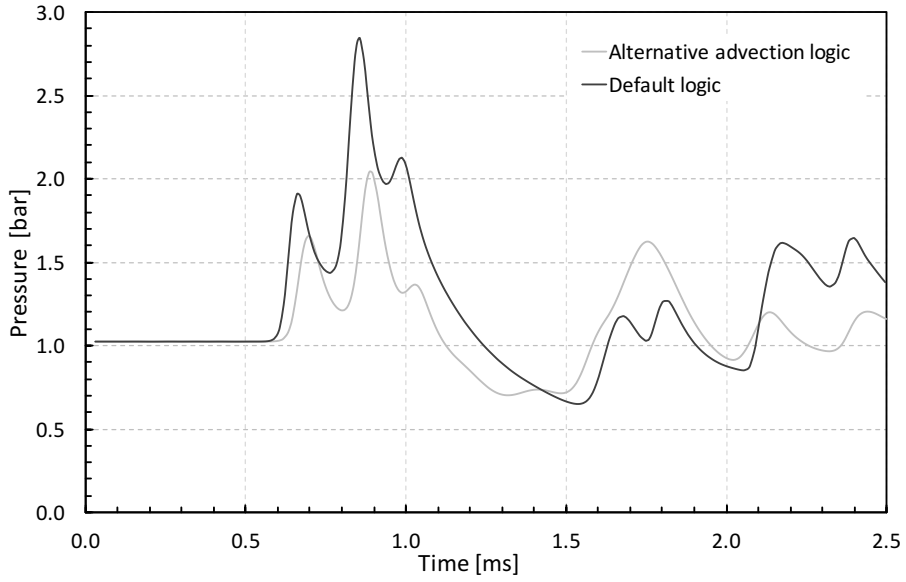

Figure 8: Comparison between two solutions, using different logics, for the confined TNT explosion described by Hu [34].

As stated above, the compartment walls were defined as rigid in all simulations. This is, however, not a good

representation of the real system as they will surely deform elastically and eventually plastically, affecting the observed peak pressure values. As such, the structure was subsequently modelled considering a suitable fluid structure interaction (FSI) technique [78]. With this added feature, the obtained pressure histories retain the generic shape but the peak pressure values are reduced by approximately 20%, as can be seen in Figure 9. Apart from this, the FSI results are qualitatively consistent and did not vary significantly when changing advection methods and logics.

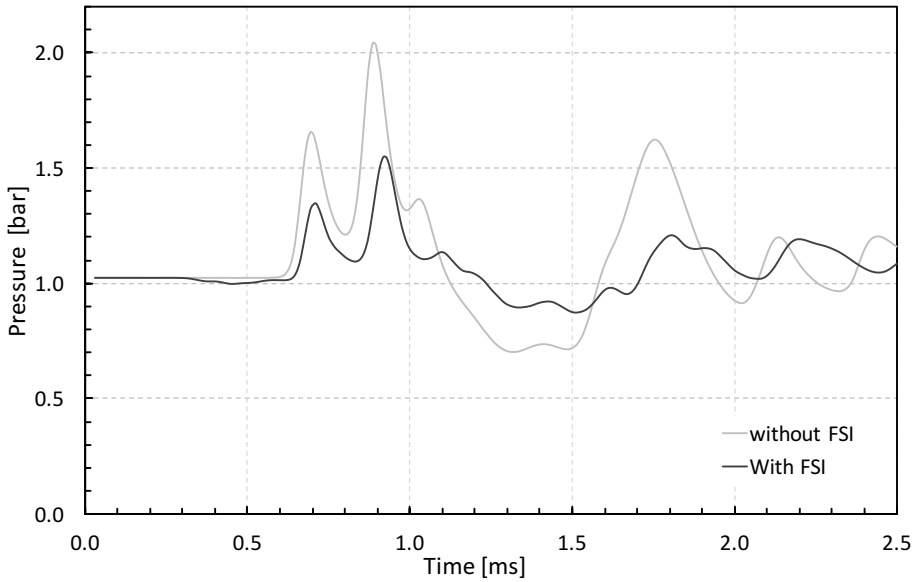

Figure 9: Comparison between the pressure at coordinates $(x, y, z) \equiv (6, 25.5, 0)$ in the confined box described by Hu [34] not using FSI and using FSI.

5. Parametric studies

5.1. The numerical models

In this section a parametric study is described where numerical simulations are used to identify how the variation in the relative dimensions of a confined space influence the maximum pressures on the interior walls. The numerical models described in the preceding sections, assessed by published experimental data, allowed the tune-up of the major modelling parameters that are now used.

Five closed rigid boxes, where one of the dimensions is kept constant and the others varied proportionally in such a way as to keep the volume constant, were subjected to the internal detonation of a fixed mass of TNT (trinitrotoluene). The volume was set equal to 2.16×10^5 cm^3 and the mass of explosive to 1.25 g. Table 5 shows the dimensions of each box, along with the number of elements used in each 3D simulation. The origin of coordinates is always located at the centre of each box and L_x, L_y and L_z are half the box sizes along each axis.

Table 5: Box dimensions and characteristics of the meshes used in the simulations

Box	Dimensions $(2L_x, 2L_y, 2L_z)$ [cm]	Number elements along (x, y, z)
1	(60, 60, 60)	(120, 120, 120)
2	(75, 60, 48)	(150, 120, 96)
3	(90, 60, 40)	(180, 120, 80)
4	(100, 60, 36)	(200, 120, 72)
5	(120, 60, 30)	(240, 120, 60)

Eight numerical simulations were performed on each box, each corresponding to a different location of the HE. The full description of the eight positions considered for each box is listed in Table 6. A comprehensive coverage of the effect of eccentric detonations inside a closed box was thus made possible.

Table 6: Location (x, y, z) of the explosive charges in each box relative to L_x, L_y and L_z.

Location	x/L_x	y/L_y	z/L_z
0	0.0	0.0	0.0
1	0.5	0.0	0.0
2	0.0	0.5	0.0
3	0.0	0.0	0.5
4	0.5	0.5	0.0
5	0.5	0.0	0.5
6	0.0	0.5	0.5
7	0.5	0.5	0.5

A set of 19 sensors was used to record the pressure histories inside the boxes, placed 5 mm away from the walls. The distribution of the sensors was the same for all simulations, as shown in Figure 10. Only one-eigth of the box was monitored, assuming that the major effects would only be observed in the close proximity of the explosive. As an example, a tabular description of the locations of the sensors for box 1 is listed in Table 7.

Only the first incident pressure peak (and the reflected pressure peak when larger than the incident) was considered in the analyses. This is assumed to be a reasonable simplification as only pressure effects were considered. It is well known, however, that impulse plays a decisive role in terms of structural response and that the reflected blast wave pressures should not be neglected as they may significantly contribute to the impulse on the compartment walls.

Input parameters were kept constant throughout the simulations and equal to those used in the validation examples. Element size was set to 5 mm. The US UFC manual [10] was also used as an additional source of validation. The average peak reflected pressure obtained from the UFC tables was 6.2 bar which compares reasonably well to the numerical result of 7.7 bar at the centre of the plate. However, the UFC manual assumes a uniform pressure load on the internal surface and does not consider wave blast reflections.

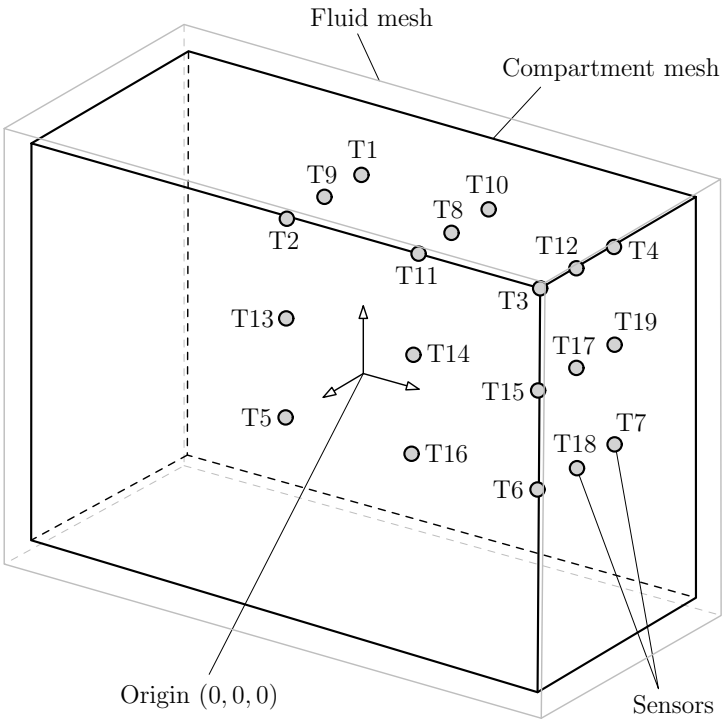

Figure 10: Positions of the sensors used to record the pressure-time curves resulting from the simulated confined explosion in each compartment.

Table 7: Location of the pressure sensors in box 1.

Sensor	x [cm]	y [cm]	z [cm]
T1	0.00	29.50	0.00
T2	0.00	29.50	29.50
T3	29.50	29.50	29.50
T4	29.50	29.50	0.00
T5	0.00	0.00	29.50
T6	29.50	0.00	29.50
T7	29.50	0.00	0.00
T8	14.75	29.50	14.75
T9	0.00	29.50	14.75
T10	14.75	29.50	0.00
T11	14.75	29.50	29.50
T12	29.50	29.50	14.75
T13	0.00	14.75	29.50
T14	14.75	14.75	29.50
T15	29.50	14.75	29.50
T16	14.75	0.00	29.50
T17	29.50	14.75	14.75
T18	29.50	0.00	14.75
T19	29.50	14.75	0.00

5.2. *Quantitative discussion of results*

The results in Figure 11 show the peak incident and the first reflected pressure values along vertical and horizontal lines passing through the wall's midpoint, illustrating the effects of a centred explosion (location 0 in Table 6) inside a cubic compartment (box 1). Note that these are not the instantaneous pressure distribution at a certain instant in time. In general a peak value is present at a point at each face, which is reduced when moving towards the edges and increases again when approaching the edges. The same is observed along the edge, such that the highest pressure values along an edge are generally observed at the corners.

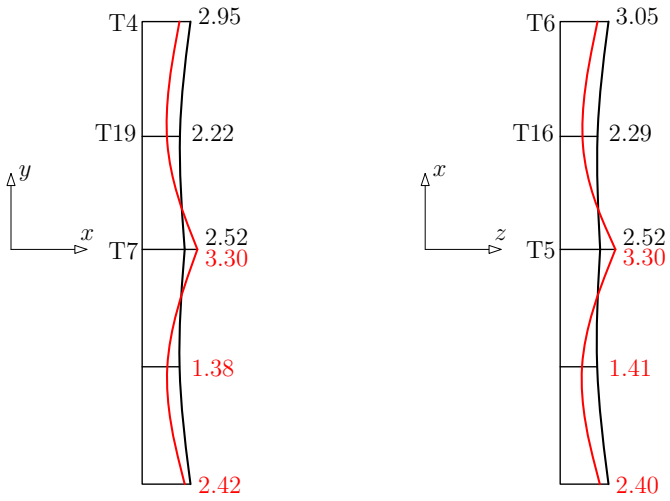

Figure 11: Profiles of incident pressure at the walls of the closed box 1 ($60 \times 60 \times 60$ [cm^3]): (a) vertical cross section of the face normal to the x axis and (b) horizontal cross section of the face normal to the y axis. The incident wave is shown in blue and the first reflected wave in red.

Analysing the time-pressure curves obtained it becomes clear that the maximum incident peak pressures are strongly dependent on the Z scaled distance. Analyses were performed to investigate possible correlations between the maximum pressure and the aspect ratio of the boxes as defined in the empirical charts of the US UFC manual [10]. However, poor correlations were obtained with all scaled parameters, other than Z.

For centred and non-centred explosions, the highest pressures in the walls were always observed at the points closer to the explosive. Nevertheless, it was verified that the confinement causes a pressure enhancement effect at corners and edges, together with complex patterns of internal blast reflexions, which in certain cases led to peak pressure values higher than in the initial blast wave. This makes pressure distribution predictions within confined spaces subjected to internal blast rather difficult.

Semi-empirical expressions, such as those proposed by Henrych [79], have been widely used for engineering purposes but were not derived to be applied to confined explosions. Nonetheless, a monotonic relation between the Z scaled distance and the incident pressure peak was observed in all the simulations. A modification of the Henrych

expression was found to give a good engineering approximation for the peak pressure results measured at the centre of all faces in the 5 boxes. This equation is

$$P = \frac{5.924}{Z} + \frac{2.941}{Z^2} + \frac{3.259}{Z^3} + \frac{0.210}{Z^4} + \frac{0.037}{Z^5} = P_{\text{walls}} \tag{15}$$

with

$$Z = \frac{R}{\sqrt[3]{W}} \tag{16}$$

where $P = P_{\text{walls}}$ [bar] is the pressure at the walls, R [m] is the stand-off distance and W [kg] is the TNT equivalent mass of high-explosive. Figure 12 shows how the new equation fits relatively well the numerical data obtained from the simulations. The original Henrych equation was also plotted giving lower peak pressures than those obtained in the numerical simulation. Since the Henrych curve has been derived for a free air explosion, this observation agrees well with reports by others [5, 10, 34] stating that the confinement enhances the internal pressures.

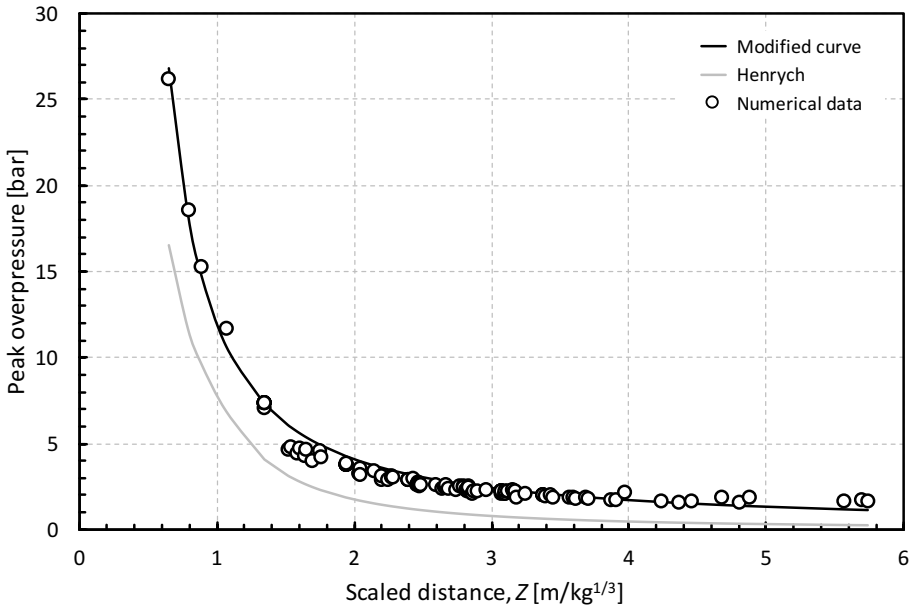

Figure 12: Maximum pressure for the first arriving blast wave: comparison between experimental data and numerical results.

Amongst other effects, engineers and designers will look for the maximum blast pressure on structures. In many cases it will not occur at the wall of the confinement but at corners and edges. Additionally, reflected waves may yield blast pressure higher than the first incident peak pressures, which again cannot be predicted by the modified formulation, or any other known method, including the UFC. However, box 1 showed a pressure focusing at the corners. The phenomenon is enhanced by blast reflexions from the internal faces which, due to the orthogonal symmetry of the

cubic shape, arrive at the same time at the opposing vertex, reinforcing each other. A value of 10.3 bar was obtained at the vertex, significantly larger than the direct overpressure of 2.52 bar impinging on the internal surfaces of the box. In fact, in many references it is assumed that the reflected blast wave pressure will decay for any subsequent wave [49] and this result shows how this assumption may deviate from reality. It was observed that the enhancement at corners and edges cannot be predicted in terms of a single parameter, such as the Z scaled distance. Reflected peak-pressures at corners are also influenced by other factors such as the angles at which the wave front arrives in relation to the faces adjacent to the corners. The maximum, minimum and average angles as well as the angular deviation from octahedral angle, assumed to be the optimum in terms of the induction blast wave mutual reinforcement, were all investigated and it was found that the maximum angle between each of the three concurrent walls at a corner and the radial stand-off distance between explosive and sensor gave the best correlation ($R^2 = 0.615$ when assuming a two degree polynomial fit). This is shown in Figure 13. The highest pressure occurs for angles ≈ 1 rad. However, as referred above, the angle alone does not explain the phenomena as for the same angle the pressure will vary significantly with the stand-off distance. The two variables were thus combined to give a rough predictor of the maximum pressure at corners. Figure 14 shows that the new predicted results are better than the single parameter modified curve from equation (15), which under-predicted most of the results. The new equation is

$$P_{\text{corner}} = 26.228 - 11.475\theta_{\max} - 1.478Z \tag{17}$$

and yields a coefficient of correlation $R^2 = 0.766$ and a standard deviation of $\sigma = 1.487$, where $\theta_{\max}$ is the maximum angle between the radial stand-off direction and the planes that contain the intersecting walls at the corner. Results in Table 8 show the highest pressure values at corner sensor T3, obtained both numerically and using the estimation equation (17). For all other boxes and explosive locations studied the pressure at corners is not represented, as there were higher pressures in other points of the box.

Equation (15) is a goof fit for the maximum pressure at the centre of the confinement walls. A closer fit was proposed for the corners in equation (17). In all other situations (edges or off-centre face points) equation (15) will underestimate the maximum peak-pressure. All these data points were aggregated as the edges only contribute with approximately 15% of the maximum peak-pressure. A new fit was derived to minimise this systematic underestimation, using equation

$$P_{\text{edge}} = 13.685Z^{-0.974} \tag{18}$$

where the independent parameter is again the Z scaled distance. The corresponding results are shown in Figure 15. The data correlation is reasonably high ($R^2 = 0.837$) and the fit is shown in Table 9. With equations (15), (17) and

Table 8: Comparison between the peak-pressures obtained numerically and using equation (17) at corner sensor T3.

Box	Location of explosive	Pressure (numerical) [bar]	Pressure (equation (17)) [bar]	Error [%]
1	0	10.3	9.92	3.7
1	7	16.4	16.01	2.4
2	0	4.76	6.24	31.0
2	1	6.00	7.62	27.0
2	4	11.6	10.88	6.2
2	7	11.8	12.59	6.7
3	1	5.57	8.09	45.0
3	4	8.24	8.96	8.7
3	7	9.43	10.04	6.5
4	4	8.75	8.77	0.2
4	7	8.98	8.70	3.1
5	7	5.82	6.34	8.9

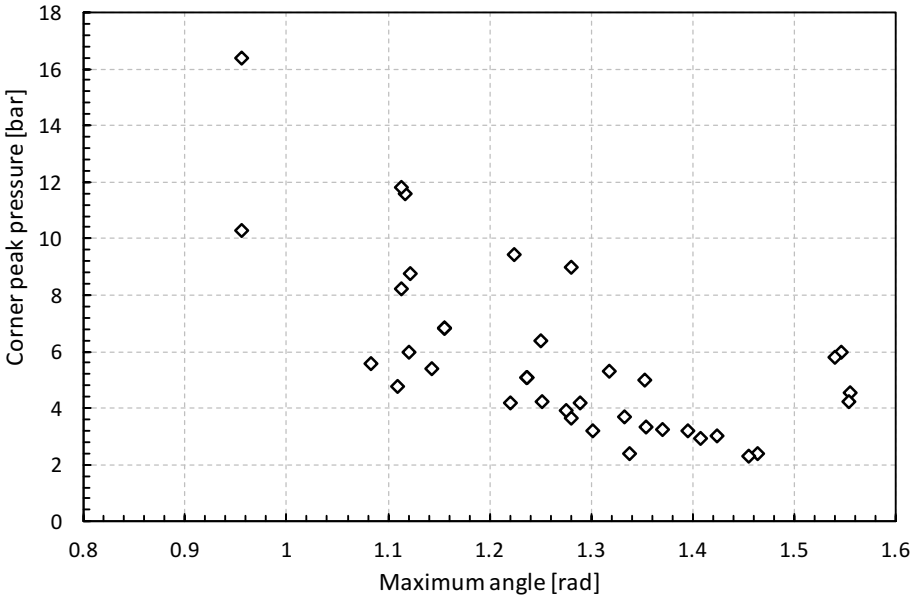

Figure 13: Peak pressure at corners as a function of the maximum angle between the corner position vector and the three coordinate axis.

(18) it is possible to cover most of the pressure distribution inside a closed unvented prismatic box.

5.3. Qualitative discussion of results

The cubic box (box 1) pressure-time curve at the wall centre is shown in Figure 16. Due to symmetry the results are the same for all faces and only one curve is represented. In this configuration the peak-pressure of the blast reflexion is higher than the direct shock wave reflected pressure. As the box shape is changed into a more slender shape (longer and narrower)) it is observed that the first blast reflexion gradually increases its strength, as can also be

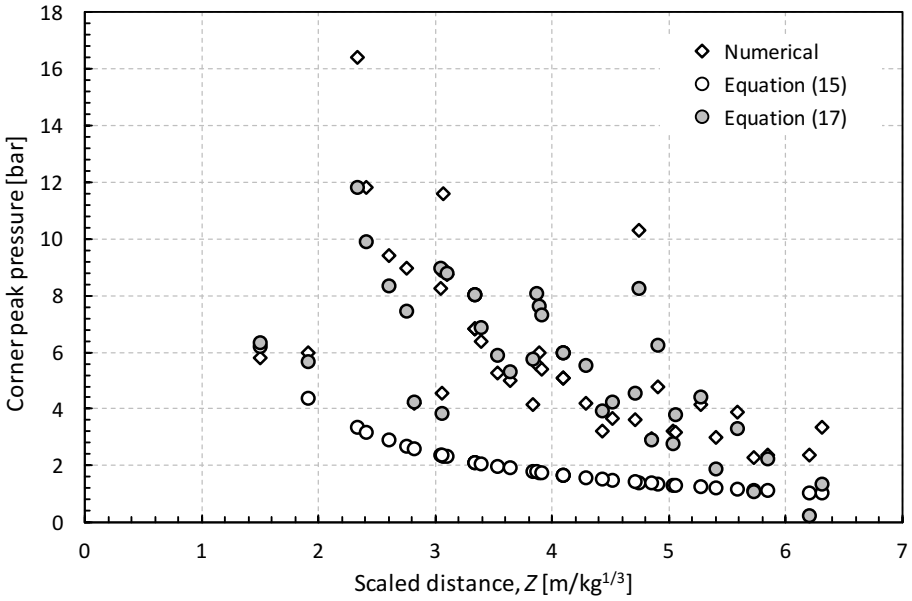

Figure 14: Comparison of the corner peak pressure results obtained numerically and predicted by equations (15) and (17).

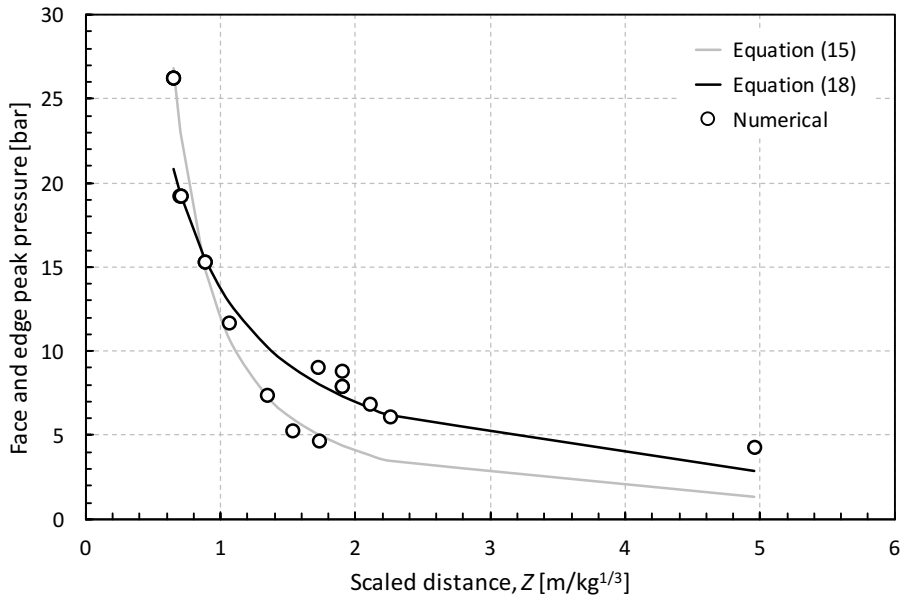

Figure 15: Comparison between the numerical results and equations (15) and (18), for peak-pressures at edges and face off-centred points.

seen in Figure 16, which shows the pressure-time curve at the face normal to the x axis for boxes 1 and 5, and at the same time the first direct peak becomes lower, due to the increased stand-off distance. The increasing slenderness ratio also favours reflexions in the longer direction. Stronger reflected blasts are observed in the centre of the face normal to x and sometimes also in the adjacent sensors T18 and T19 (see Figure 10) for those cases where the explosive

Table 9: Comparison between the peak-pressures obtained numerically and from equation (18).

Box	Location of explosive	Z [m/kg$^{1/3}$]	Sensor point	Pressure (numerical) [bar]	Pressure (equation (18)) [bar]	Error [%]
1	4	1.90	4	8.78	7.31	16.7
2	2	1.73	9	4.64	8.01	72.6
2	4	1.07	16	11.7	12.84	9.7
2	6	1.72	2	9.06	8.08	10.8
3	0	4.96	4	4.28	2.88	32.7
3	2	2.26	2	6.12	6.20	1.3
3	5	0.88	16	15.3	15.47	1.11
3	6	0.88	13	15.3	15.47	1.11
3	7	0.88	14	15.3	15.47	1.11
4	1	1.53	16	5.24	9.02	72.1
4	2	2.11	2	6.81	6.61	2.9
4	5	0.70	16	19.2	19.3	0.5
4	6	0.70	13	19.2	19.3	0.5
4	7	0.70	14	19.2	19.3	0.5
5	1	1.35	16	7.41	10.24	38.2
5	2	1.90	2	7.88	7.31	7.2
5	4	1.90	11	7.88	7.31	7.2
5	5	0.65	16	26.2	20.82	20.5
5	6	0.65	13	26.2	20.82	20.5
5	7	0.65	14	26.2	20.82	20.5

is moved to a position in front of those points (respectively locations 5 and 6 in Table 6). In the other directions the gradually shorter stand-off distance along the z direction explains the rapid increase of the peak-pressure in the faces normal to z while the peak values do not change significantly along the y direction, whose width has been kept constant. At the vertex a strong reflexion is observed due to the simultaneously arrival of reflexions from all the three orthogonal directions. Even for non-cubic boxes the wave reinforcement is evident as shown in Figure 17 showing the pressure distribution pattern at a certain time of the simulation, where the corners of the box nearer to the explosive are experiencing the largest pressures.

As the explosive is moved from its central position the phenomena becomes more difficult to understand but the shortest stand-off will generally dictate the highest peak-pressure. A better correlation was obtained at corners by considering the influence of the angles between the line of sight from the explosive to the sensor and the main coordinate axis. The highest magnitude pressure peaks were observed for maximum angles close to 1 rad. Interestingly, as the distance to the z face diminishes the location of the peak pressure moves from the centre of the face to the edge (T2), where the stand-off distance is larger. Three major observations emerged from the analysis: (i) as the compartment becomes more slender the blast reflexions in the longer direction become more significant than the direct blasts; (ii) as the transverse dimension, i.e. the width, diminishes the edges will experience higher pressure than the faces perpen-

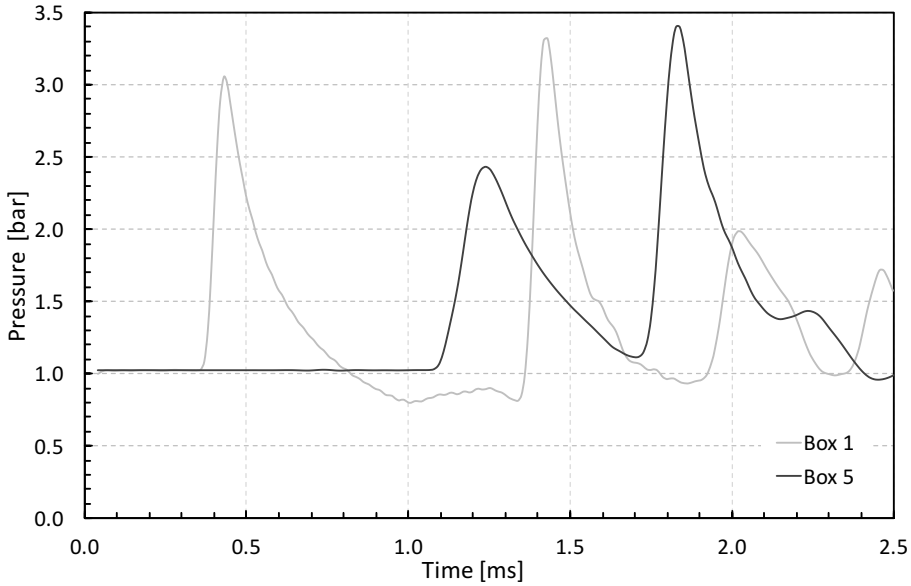

Figure 16: Pressure-time history at the centre of the faces normal to x for boxes 1 and 5 (using FSI).

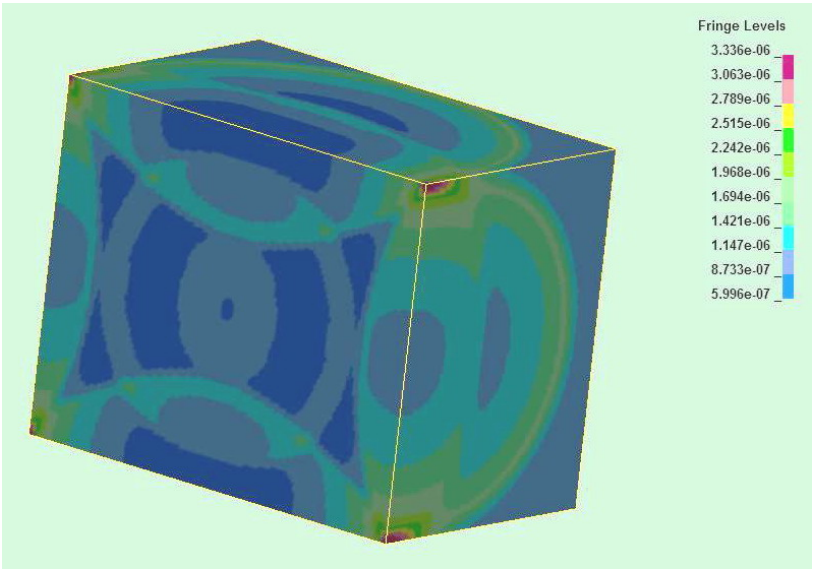

Figure 17: Reflected wave pressure peak at corner (tracer point 3) for box 2 with explosive located half way between the centre of the box and the face normal to the z axis.

dicular to the width; and (iii) symmetry induces an increase in corner pressure. In the remaining positions pressure will depend mostly on the stand-off distance. The maximum pressure in all boxes and for all explosive locations are listed in Table 10. It can be seen that in many cases the reflexions yielded pressures lower than the first direct peaks.

Table 10: Maximum recorded peak pressures for different locations of the explosive and different boxes.

Location of explosive	Box	Z [m/kg$^{1/3}$]	Direct blast P_{max} [bar] (sensor)	Reflected blast P_{max} [bar] (sensor)
1	0	4.74	4.80 (3)	10.3 (3)
1	1	1.35	7.47 (7)	3.39 (11)
1	4	1.90	8.78 (4)	2.55 (14)
1	7	2.33	16.4 (3)	
2	0	4.90	4.76 (3)	3.72 (4)
2	1	3.89	6.00 (3)	
2	2	1.35	8.00 (1)	2.37 (19)
2	3	1.07	11.7 (5)	4.17 (3)
2	4	2.16	11.6 (3)	
2	5	1.07	11.7 (16)	
2	6	1.72	9.06 (2)	
2	7	1.72	11.8 (3)	
3	0	1.81	5.24 (5)	3.58 (6)
3	1	3.87	5.57 (3)	
3	2	2.26	6.12 (2)	2.30 (7)
3	3	0.88	15.3 (5)	2.58 (18)
3	4	3.04	8.24 (3)	
3	5	0.88	15.3 (16)	3.35 (18)
3	6	0.88	15.3 (13)	1.87 (19)
3	7	0.88	15.3 (14)	
4	0	1.62	6.61 (5)	3.24 (1)
4	1	3.91	5.40 (3)	2.26 (1)
4	2	2.11	6.81 (2)	2.10 (19)
4	3	0.79	19.2 (5)	2.46 (18)
4	4	3.10	8.75 (3)	3.36 (7)
4	5	0.70	19.2 (16)	2.85 (18)
4	6	0.70	19.2 (13)	
4	7	0.70	19.2 (14)	
5	0	1.35	8.14 (5)	3.40 (7)
5	1	1.35	7.41 (16)	4.22 (7)
5	2	1.90	7.88 (2)	1.95 (6)
5	3	0.65	26.2 (5)	2.80 (6)
5	4	1.90	7.88 (11)	3.75 (19)
5	5	0.65	26.2 (16)	
5	6	0.65	26.2 (13)	
5	7	0.65	26.2 (14)	

6. The afterburning effects

TNT is strongly oxygen deficient (73.9%) which means that in its detonation phase some of its constituents will remain unreacted due to insufficient oxygen in the composition. As a consequence, a secondary combustion will take place if conditions arise that allow them to react later with atmospheric oxygen. This reaction can be either complete or partial depending on the the available amount of oxygen. For a full afterburning of a TNT charge, the ratio of the explosive mass to the volume of the confinement W/V shall be lower than 0.387 kg/m^3 [56]. For the boxes

considered in the present analysis $W/V = 0.0058$ kg/m^3, which means that the volume of air available is nearly 70 times higher than the stoichiometric ratio. According to Salzano and Basco [53], for such a low W/V ratio the effect of the afterburning phenomenon becomes relatively small. The same conclusion can be obtained from Feldgun et al. [56] who plotted gas pressure versus W/V curves obtained from experimental results, from the UFC-3-340 manual [10] and from the Jones-Wilkins-Lee (JWL) equation of state, which can be written as [56]

$$P = \left[\frac{P_0}{\gamma_0 - 1}(V - V_E) + E\rho_E V_E\right]\frac{\omega^2}{\theta V} + A\left(1 - \frac{\omega}{R_1\theta}\right)e^{-R_1\theta} + B\left(1 - \frac{\omega}{R_2\theta}\right)e^{-R_2\theta} \tag{19}$$

where V and V_E are the current and initial volumes of the explosive, ρ_E and ρ_0 are the explosive and initial air densities, P_0 is the initial ambient pressure, E is the internal energy of the explosion, $\theta = V/V_E$, $\omega = \gamma - 1$ and γ is the heat capacity ratio of the explosive. The coefficients A, B, R_1 and R_2 are empirical parameters which depend on the explosive's formulation. A plot of such curves is presented in Figure 18, which is based on the UFC manual [10] and the work of Feldgun et al. [56]. For $W/V = 0.0058$ kg/m^3 the gas pressure yields approximately 0.4 bar. This is most probably due to the fact that the large relative volume of the box does not favour the necessary heating of the detonation products. This is also confirmed by a plot of gaseous temperature versus W/V, presented by Edri [54], where a W/V ratio of 0.0058 gives a temperature lower than 500 K, which is significantly lower than the required 900 K.

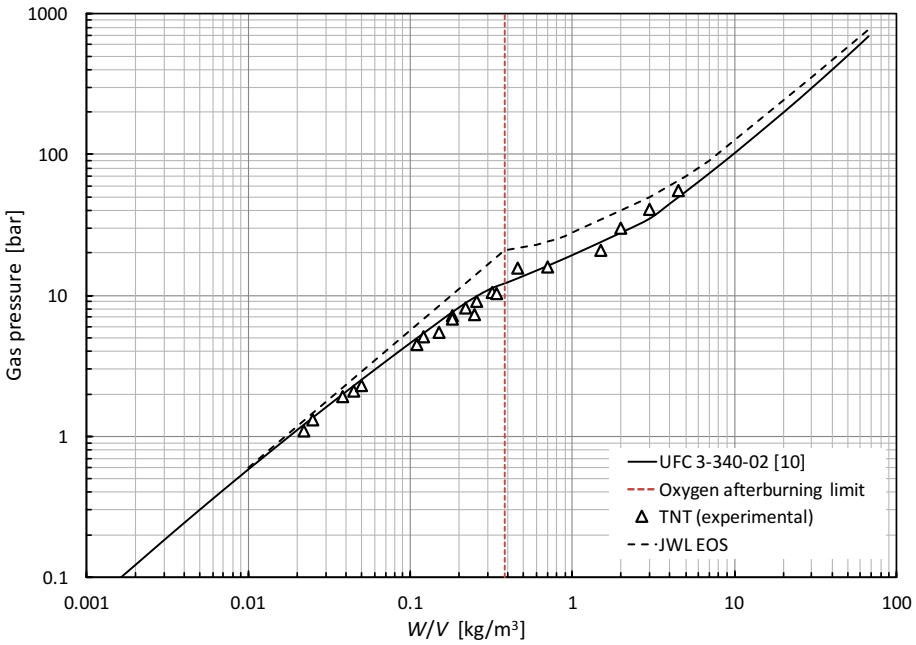

Figure 18: Gas pressures obtained from experimental data, the JWL equation of state (equation 19) and the UFC manual (adapted from [56]).

One other relevant aspect to this discussion is the time of initiation of the afterburning effect. Even if reactants and oxygen are present, a good mixing of these and a sufficiently high temperature will be required to enable the reaction to occur. This starting time has been suggested to be the time when the first reflexion of the detonation wave interacts with the detonation products rising its temperature and providing a good mixing with air [55, 57]. As such, afterburning will start a few milliseconds after the initial detonation, which means that the first shock-wave and its first reflexion will not be affected by the phenomenon. Its effects on the subsequent internal pressures can be estimated by using the approach suggested by Edri et al. [54], which considers a shift of the pressure-time history related to the ratio of the total explosive reaction energy to the detonation energy, t_s, as shown in

$$P(t)_{\text{shifted}} = P(t) + P_g(K_{ab} - 1) \tag{20}$$

where $P(t)_{\text{shifted}}$ is the pressure time curve with consideration of afterburn, $P(t)$ is the pressure-time curve obtained without considering afterburning, P_g is the residual gas pressure and $K_{ab} = E_{\text{tot}}/E_{\text{det}}$ is the ratio of the total energy of the explosion to the heat of detonation. The authors reported a good agreement with experimental data by using this simple approach [54]. For a full afterburning of TNT this ratio is about 3.22 times the heat of detonation and using this approach for a gas pressure of about 0.4 bar the pressure shift is approximately 0.89 bar.

As discussed above, the majority of the peak overpressures computed in this work resulted from the first shock wave and its reflexions. Even if the few second and third peaks that were computed throughout the analyses were to suffer such a pressure increase this would not substantially change the derived results. Therefore, it is considered that for such a low W/V ratio the effect of afterburning can be neglected for the purpose of the present study.

7. Concluding remarks

The validation studies showed that it is possible to obtain reasonably accurate numerical solutions for confined explosions by using the ALE methodology. However, the choice of input parameters is strongly dependent on the specific case being analysed. As such, it is still difficult to define recommendations regarding the input of parameters for an ALE simulation of an arbitrary confined explosion. The present numerical calculations were performed with LS-DYNA and some of the parameters mentioned are specific for this hydrocode. Nonetheless, in general terms, hydrocode users should carefully judge the choice of the simulation parameters available as guidance on this choice only comes from experience or available experimental data to compare with.

It was observed that the direct shock wave reflected peak-pressure at the centre of unvented prismatic confinement walls, subject to an internal explosion, can be reasonably well predicted in terms of the stand-off distance using

the modified equation (15), which is based on the work of Henrych [79]. Subsequent reflexions are more complex to understand but in general their pressure intensity is lower than the first blast. Traditional empirical assumptions regarding the decay of the reflected pressure peaks in the enclosure [49] may, in a number of cases, not correspond to reality, particularly for slender compartments where reflected peaks tend to be more intense. The angle between the stand-off direction and the main planes of the internal faces of the box correlates reasonably with the peak-pressures obtained at the corners. It is believed that these angles will contribute to the pressure enhancement effect observed in certain cases, which could not be explained by the stand-off or z scaled distance alone. Equation (17) is a fit for the maximum pressure at corners. It was found that, for all other locations, a better description of the peak-pressures could be obtained using equation (18).

It was also observed that for pressure analyses the contribution of blast reflexions is relatively unimportant although results show that in many cases reflexions may show higher pressure peaks than the first arriving waves.

Afterburning has been discussed but its relevance was considered unimportant for the present study since the ratio of explosive mass and volume of air is very small, which means that the detonation products will cool rapidly and the resulting gas pressure will be small when compared with the obtained peak overpressures. However, the contribution to the resulting impulse may be relavant, although this was outside the scope of this work.

Acknowledgements

Author João B. Cardoso greatly acknowledges the financial support of the Portuguese Foundation for Science and Technology (FCT), through UNIDEMI, under the Strategic Project UID/EMS/00667/2013.

References

[1] C.N. Kingery, G.A. Coulter. *Reflected overpressure impulse on a finite structure*, Technical Report ARBRL-TR-02537, Ballistic Research Laboratory, Aberdeen, Maryland, 1983.

[2] P.W. Gibson. *Blast overpressure and survivability calculations*, Technical Report NATICK/TR-95/003, US Army Natick Research, Development and Engineering Center, Massachusetts, 1994.

[3] A.M. Remennikov. *A Review of methods for predicting bomb blast effects on buildings*, URL: http://ro.uow.edu.au/engpapers/357, 2003.

[4] B.M. Luccioni, R.D. Ambrosini, R.F. Danesi, J.B. Tera. Analysis of building collapse under blast loads, *Eng. Struct.* **26**:63-71, 2004.

[5] A.M. Remennikov, T.A. Rose. Modelling blast loads on buildings in complex city geometries, *Comput. Struct.* **83**(27):2197-2205, 2005.

[6] P. Sherkar, A.S. Whittaker, A.J. Aref. *Modeling the effects of detonations of high explosives to inform blast-resistant design*, Technical Report MCEER-10-0009, Multidisciplinary Center for Earthquake Engineering Research, Bufalo, New York, 2010.

[7] M. Silvestrini, B. Genova, F.J. Leon Trujillo. Energy concentration factor: A simple concept for the prediction of blast propagation in partially confined geometries, *J. Loss Prev. Process Ind.* **22**(4):449-454, 2009.

[8] T. Krauthammer. *Modern Protective Structures*, vol. 22. CRC Press, 2008.

[9] G. Randers-Pehrson, K.A. Bannister. *Airblast loading model for DYNA2D and DYNA3D*, Technical Report ARL-TR-1310, Army Research Laboratory, 1997.

[10] *Unified Facilities Criteria (UFC 3-340-03). Structures to resist the effect of accidental explosions*, US Department of Defense Tri-Series Manual, 2014.

[11] G.F. Kinney, R.G. Sewell, K.J. Graham. *Peak overpressures for internal blast*, Technical Report NWC-TP-6089, Naval Weapons Center, China Lake, California, 1979.

[12] W.E. Baker, C.E. Anderson Jr, B.L. Morris, D.K. Vauters. Quasi-Static pressure, duration and impulse for explosions in structures, *Int. J. Mech. Sci.* **25**:455-464, 1983.

[13] E.D. Esparza, W.E. Baker, G.A. Oldham. *Blast pressures inside and outside suppressive structures*, Technical Report EM-CR-76042, Southwest Research Institute, San Antonio, Texas, 1975.

[14] W.E. Baker, P.S. Westine. *Methods of predicting blast loads inside and blast fields outside suppressive structures*, Technical Report EM-CR-76026, Southwest Research Institute, San Antonio, Texas, 1975.

[15] W.E. Baker, G.A. Oldham. *Estimates of blowdown of quasi-static pressures in vented chambers*, Technical Report EM-CR-76029, Southwest Research Institute, San Antonio, Texas, 1975.

[16] C. Kingery, R. Schumacher, W. Ewing Jr. *Internal pressure from explosions in suppressive structures*, Technical Report ARBRL-MR-02848, Ballistic Research Laboratory, Aberdeen, Maryland, 1978.

[17] E. Strønsøe. *Calculation of pressure and temperature from explosions in confined spaces*, Technical Report ADA059840, Norwegian Defence Research Establishment, Kjeller, Norway, 1978.

[18] W.A. Keenan, J.E. Tancreto. *Design criteria for frangible covers in ordnance facilities*, Technical Report AD P000438, Naval Civil Engineering Laboratory, Port Huneme, California, 1982.

[19] C. Kingery. *Survey of airblast data related to underground storage sites*, Technical Report BRL-TR-3012, Ballistic Research Laboratory, Aberdeen, Maryland, 1989.

[20] D.M. Razus, U. Krause. Comparison of empirical and semi-empirical calculation methods for venting of gas explosions, *Fire Saf. J.* **36**(1):1-23, 2001.

[21] F. Tamanini. Scaling parameters for vented gas and dust explosions, *J. Loss Prev. Process Ind.* **14**(6):455-461, 2001.

[22] V.V. Molkov, A.V. Grigorash, R.M. Eber. Vented gaseous deflagrations: Modelling of spring-loaded inertial vent covers, *Fire Saf. J.* **40**(4):307-319, 2005.

[23] V.V. Molkov, R. M. Eber, A.V. Grigorash, F. Tamanini, R. Dobashi. Vented gaseous deflagrations: modelling of translating inertial vent covers, *J. Loss Prev. Process Ind.* **16**(5):395-402, 2003.

[24] V.V Molkov, A.V. Grigorash, R.M. Eber, D.V. Makarov. Vented gaseous deflagrations modelling of hinged inertial vent covers, *J. Hazard. Mater.* **116**(1-2):1-10, 2004.

[25] I. Edri, Z. Savir, V.R. Feldgun, Y.S. Karinski, D.Z. Yankelevsky. On blast pressure analysis due to a partially confined explosion: I. Experimental studies, *Int. J. Prot. Struct.* **2**(1):1-20, 2011.

[26] J.F. Proctor, W.S. Filler. *A computerized technique for blast loads from confined explosions*, in 14th Annual Explosives Safety Seminar, New Orleans, 1972.

[27] P.E. Montanaro, M.M. Swisdak Jr. *INBLAST — A New and Revised Computer Code for the Prediction of Blast Inside Closed or Vented Structures*, Silver Spring, MD, 1990.

[28] J.E. Tancreto, W.H.Z. Zehrt Jr. *Design for internal quasi-static pressures from partially confined explosions*, in 28th Department of Defense Explosive Safety Seminar, Orlando, 1998.

[29] D.K. Pritchard, D.J. Freeman, P.W. Guilbert. Prediction of explosion in confined spaces pressures, *J. Loss Prev. Process Ind.* **9**(3):205-215, 1996.

[30] G. Ferrara, A. Di Benedetto, E. Salzano, G. Russo. CFD analysis of gas explosions vented through relief pipes, *J. Hazard. Mater.* **137**(2):654-65, 2006.

[31] F. Rigas, S. Sklavounos. Experimentally validated 3-D simulation of shock waves generated by dense explosives in confined complex geometries, *J. Hazard. Mater.* **121**(1-3):23-30, 2005.

[32] W. He, J. Chen, J. Guo. Dynamic analysis of subway station subjected to internal blast loading, *J. Cent. South Univ. Technol.* **18**(3):917-924, 2011.

[33] P.C. Chan, H.H. Klein. A Study of blast effects inside an enclosure, *J. Fluids Eng.* **116**:450-455, 1994.

[34] Y. Hu, C. Wu, M. Lukaszewicz, J. Dragos, J. Ren, M. Haskett. Characteristics of confined blast loading in unvented structures, *Int. J. Prot. Struct.* **2**(1):21-44, 2011.

[35] P.E. Sauvan, I. Sochet, S. Trélat. Analysis of reflected blast wave pressure profiles in a confined room, *Shock Waves* **22**(3):253-264, 2012.

[36] Z. Whenhui, X. Honglu, Z. Guangquan, G.K. Schleyer. Dynamic response of cylindrical explosive chambers to internal blast loading produced by a concentrated charge, *Int. J. Impact Eng.* **19**(97):831-845, 1997.

[37] F. Auslender, A. Combescure. Spherical elastic-plastic structures under internal explosion. Approximate analytical solutions and applications, *Eng. Struct.* **22**:984-992, 2000.

[38] T.A. Duffey, C. Romero. Strain growth in spherical explosive chambers subjected to internal blast loading, *Int. J. Impact Eng.* **28**(9):967-983, 2003.

[39] C. Wu, M. Lukaszewicz, K. Schebella, L. Antanovskii. Experimental and numerical investigation of confined explosion in a blast chamber, *J. Loss Prev. Process Ind.* **26**(4):737-750, 2013.

[40] G.S. Langdon, A. Ozinsky, S. Chung Kim Yuen. The response of partially confined right circular stainless steel cylinders to internal air-blast loading, *Int. J. Impact Eng.* **73**:1-14, 2014.

[41] L. Ma, J. Xin, Y. Hu, J. Zheng. Ductile and brittle failure assessment of containment vessels subjected to internal blast loading, *Int. J. Impact Eng.* **52**:28-36, 2013.

[42] J. Karnesky, P. Chatterjee, F. Tamanini, S. Dorofeev. An application of 3D gasdynamic modeling for the prediction of overpressures in vented enclosures, *J. Loss Prev. Process Ind.* **20**(4-6):447-454, 2007.

[43] G. Ferrara, S.K. Willacy, H.N. Phylaktou, G.E. Andrews, A. di Benedetto, E. Salzano, G. Russo. Venting of gas explosion through relief ducts: interaction between internal and external explosions, *J. Hazard. Mater.* **155**(1-2):358-68, 2008.

[44] D.J. Park, Y.S. Lee, A.R. Green. Prediction for vented explosions in chambers with multiple obstacles, *J. Hazard. Mater.* **155**(1-2):183-92, 2008.

[45] D.J. Park, Y.S. Lee, A.R. Green. Experiments on the effects of multiple obstacles in vented explosion chambers, *J. Hazard. Mater.* **153**(1-2):340-50, 2008.

[46] A.M. Remennikov, T.A. Rose. Modelling blast loads on buildings in complex city geometries, *Comput. Struct.* **83**(27):2197-2205, 2005.

[47] S. Sklavounos, F. Rigas. Computer simulation of shock waves transmission in obstructed terrains, *J. Loss Prev. Process Ind.* **17**(6):407-417, 2004.

[48] C. Geretto, S. Chung Kim Yuen, G.N. Nurick. An experimental study of the effects of degrees of confinement on the response of square mild steel plates subjected to blast loading, *Int. J. Impact Eng.* **79**:32-44, 2015.

[49] J. Dragos, C. Wu, D.J. Oehlers. Simplification of fully confined blasts for structural response analysis, *Eng. Struct.* **56**:312-326, 2013.

[50] A.M. Benselama, M.J.-P. William-Louis, F. Monnoyer. A 1D-3D mixed method for the numerical simulation of blast waves in confined

geometries, *J. Comput. Phys.* **228**(18):6796-6810, 2009.

[51] A. Zyskowski, I. Sochet, G. Mavrot, P. Bailly, J. Renard. Study of the explosion process in a small scale experiment-structural loading, *J. Loss Prev. Process Ind.* **17**(4):291-299, 2004.

[52] C. Price, J.A. Sherburn, D. Nelson, T. Slawson, R.N. Boone. Evaluation of predictive methods for airblast propagation through an enclosed structure, *Int. J. Prot. Struct.* **2**(1):71-82, 2011.

[53] E. Salzano, A. Basco, Comparison of the explosion thermodynamics of TNT and black powder using Le Chatelier diagrams, *Propell., Explos., Pyrot.* **37**:724-731, 2012.

[54] I. Edri, V.R. Feldgun, Y.S. Karinski, D.Z. Yankelevsky, Afterburning aspects of an internal TNT explosion, *Int. J. Prot. Struct.* **4**(1):97-116, 2013.

[55] I. Edri I, V.R. Feldgun, Y.S. Karinski, D.Z. Yankelevsky, On blast pressure analysis due to a partially confined explosion: III. Afterburn effect, *Int. J. Prot. Struct.* **3**(3):311-331, 2012.

[56] V.R. Feldgun, Y.S. Karinski, I. Edri, D.Z. Yankelevsky, Prediction of the quasi-static pressure in confined and partially confined explosions and its application to blast response simulation of flexible structures, *Int. J. Impact Eng.* **90**:46-60, 2016.

[57] L.E. Schwer, *Jones-Wilkins-Lee (JWL) equation of state with afterburning*, in Proc. of the 14th International LS-DYNA Users Conference, pp. 1-38, 2016.

[58] A.L. Kuhl, M. Howard, L. Fried, *Thermodynamic model of afterburning in explosives*, in Proc. of the 34th International ICT Conference: Energetic Materials: Reactions of Propellants, Explosives and Pyrothecnics, Karlsruhe, Germany, 2003.

[59] D.L. Ornellas, *Calorimetric determinations of the heat and products of detonation for explosives: October 1961 to April 1982*, Report UCRL-52821, Lawrence Livermore National Laboratory, Livermore CA, 1982.

[60] P.W. Cooper, *Explosives engineering*, Wiley-VCH, Toronto, 1996.

[61] L.E. Fried, P.C. Souers, *Cheetah 2.0: User's Manual*, Lawrence Livermore National Laboratory, Livermore CA, 1998.

[62] S. Gordon, B.J. McBride, *Computer program for calculation of complex chemical equilibrium compositions and applications*, Report NASA RP 1311, Washington D.C., USA, 1994.

[63] J.A. Zukas, *Introduction to Hydrocodes*, Studies in Applied Mechanics, Elsevier, 2004.

[64] T.J.R. Hughes, W.K. Liu, T.K. Zimmermann. Lagrangian-Eulerian finite element formulation for incompressible viscous flows, *Comput. Methods Appl. Mech. Eng.* **29**:329-349, 1981.

[65] D. Benson. *Computational methods in Lagrangian and Eulerian hydrocodes*, *Comput. Meth. Appl. Mech. Eng.* **99**(2-3):235-314, 1992.

[66] D.J. Benson. A multi-material Eulerian formulation for the efficient solution of impact and penetration problems, *Comput. Mech.* **15**:558-571, 1995.

[67] T. Belytschko, W.K. Liu, B. Moran. *Nonlinear finite elements for continua and structures*, Wiley, Chichester, 2000.

[68] A. Alia, M. Souli. High explosive simulation using multi-material formulations, *Appl. Therm. Eng.* **26**(10):1032-1042, 2006.

[69] S. K. Godunov. Finite difference methods for numerical computation of discontinuous solutions of the equations of fluid dynamics, *Matematichskii Sbornik* **47**(3):271-306, 1959.

[70] V. Leer. Towards the Ultimate Conservative Difference Scheme. IV. A New Approach to Numerical Convection, *J. Comput. Phys.* **167**:276-299, 1977.

[71] D.J. Benson. Computational methods in Lagrangian and Eulerian hydrocodes, *Comput. Methods Appl. Mech. Eng.* **99**:235-394, 1992.

[72] E.L. Lee, H.C. Horning, J.W. Kury. *Adiabatic expansion of high explosives detonation products*, Technical Report TID 4500-UCRL 50422, Lawrence Livermore National Laboratory, University of California, 1968.

[73] S. Grys, W.A. Trzcinski. Calculation of combustion, explosion and detonation characteristics of energetic materials, *Cent. Eur. J. Energ.*

Mater. **7**(2):pp. 97-113, 2010.

[74] N. Aquelet, M. Souli. *2D to 3D ALE Mapping*, in Proc. of the 10th International LS-DYNA Users Conference, pp. 15-24, 2008.

[75] M. Larcher. *Simulation of the Effects of an Air Blast Wave*, Joint Research Centre (JRC), European Comission, 2007.

[76] J.A. Zukas, D.R. Scheffler. Practical aspects in numerical simulation of dynamic events — Effects of meshing, *Int. J. Impact Eng.* **24**:925-945, 2000.

[77] K. Mahmadi, N. Aquelet. Delayed mesh relaxation for multi-material ALE formulation, *Int. J. Heat Fluid Flow* **46**:102-111, 2014.

[78] M.S. Chafi, G. Karami, M. Ziejewski. Numerical analysis of blast-induced wave propagation using FSI and ALE multi-material formulations, *Int. J. Impact Eng.* **36**(10-11):1269-1275, 2009.

[79] J. Henrych. *The dynamics of explosion and its use*, Elsevier, 1979.